Cell Stem Cell

Resource

The landscape of drug sensitivity and resistance in sarcoma

Graphical abstract

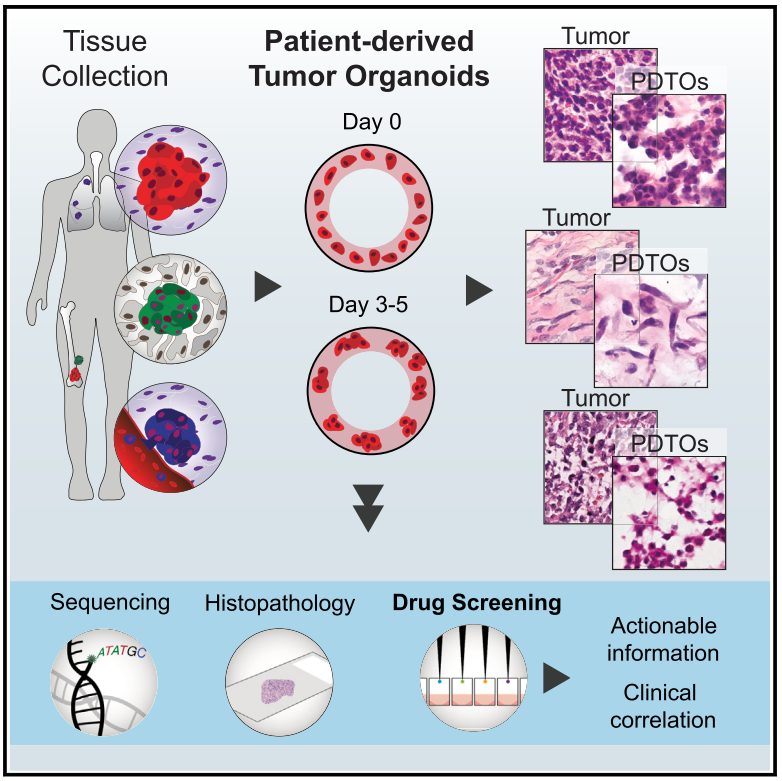

Authors

Ahmad Al Shihabi, Peyton J. Tebon, Huyen Thi Lam Nguyen, ..., Noah C. Federman, Jane Yanagawa, Alice Soragni

Correspondence

alices@mednet.ucla.edu

In brief

Al Shihabi et al. employ patient-derived tumor organoids from >110 specimens to study drug sensitivity and resistance across 21 sarcoma types. They find patient- and subtype-specific responses, correlating with clinical features and outcomes. They identified actionable regimens for most samples, highlighting the potential of organoids for functional precision medicine applications.

Highlights

- Standardized organoid culture preserves unique sarcoma histopathological features
- Drug screening on organoids yields sensitivity info correlating with clinical features
- Organoid response to treatment correlates with patient therapy outcomes
- Scalable functional precision medicine programs are feasible in a single institution

Al Shihabi et al., 2024, Cell Stem Cell *31*, 1524–1542
October 3, 2024
https://doi.org/10.1016/j.stem.2024.08.010

CellPress

CellPress
OPEN ACCESS

Cell Stem Cell

Resource

The landscape of drug sensitivity and resistance in sarcoma

Ahmad Al Shihabi,[1,2,17] Peyton J. Tebon,[1,3,17] Huyen Thi Lam Nguyen,[1,17] Jomjit Chantharasamee,[4,16] Sara Sartini,[1] Ardalan Davarifar,[1,4,5] Alexandra Y. Jensen,[1] Miranda Diaz-Infante,[1] Hannah Cox,[1] Alfredo Enrique Gonzalez,[5] Summer Norris,[1] Jantzen Sperry,[6] Jonathan Nakashima,[6] Nasrin Tavanaie,[1] Helena Winata,[5] Sorel T. Fitz-Gibbon,[5] Takafumi N. Yamaguchi,[5] Jae H. Jeong,[5] Sarah Dry,[2] Arun S. Singh,[4] Bartosz Chmielowski,[4] Joseph G. Crompton,[7,8] Anusha K. Kalbasi,[9] Fritz C. Eilber,[8] Francis Hornicek,[10] Nicholas M. Bernthal,[1] Scott D. Nelson,[2] Paul C. Boutros,[5,7,11,12,13] Noah C. Federman,[1,7,14] Jane Yanagawa,[15] and Alice Soragni[1,7,12,18,*]

[1]Department of Orthopaedic Surgery, David Geffen School of Medicine, University of California, Los Angeles, Los Angeles, CA, USA
[2]Department of Pathology, David Geffen School of Medicine, University of California, Los Angeles, Los Angeles, CA, USA
[3]Department of Bioengineering, University of California, Los Angeles, Los Angeles, CA, USA
[4]Division of Hematology-Oncology, David Geffen School of Medicine, University of California, Los Angeles, Los Angeles, CA, USA
[5]Department of Human Genetics, University of California, Los Angeles, Los Angeles, CA, USA
[6]Certis Oncology Solutions, Inc., San Diego, CA, USA
[7]Jonsson Comprehensive Cancer Center, University of California, Los Angeles, Los Angeles, CA, USA
[8]Division of Surgical Oncology David Geffen School of Medicine, University of California, Los Angeles, Los Angeles, CA, USA
[9]Department of Radiation Oncology, University of California, Los Angeles, Los Angeles, CA, USA
[10]Department of Orthopedic Surgery, University of Miami, Miami, FL, USA
[11]Institute for Precision Health, University of California, Los Angeles, Los Angeles, CA, USA
[12]Eli and Edythe Broad Center of Regenerative Medicine and Stem Cell Research, University of California, Los Angeles, Los Angeles, CA, USA
[13]Department of Urology, University of California, Los Angeles, Los Angeles, CA, USA
[14]Department of Pediatrics, David Geffen School of Medicine, University of California, Los Angeles, Los Angeles, CA, USA
[15]Department of Surgery, Division of Thoracic Surgery, David Geffen School of Medicine, University of California, Los Angeles, Los Angeles, CA, USA
[16]Present address: Division of Oncology, Department of Medicine, Faculty of Medicine, Siriraj Hospital, Mahidol University, Bangkok, Thailand
[17]These authors contributed equally
[18]Lead contact
*Correspondence: alices@mednet.ucla.edu
https://doi.org/10.1016/j.stem.2024.08.010

SUMMARY

Sarcomas are rare malignancies with over 100 distinct histological subtypes. Their rarity and heterogeneity pose significant challenges to identifying effective therapies, and approved regimens show varied responses. Novel, personalized approaches to therapy are needed to improve patient outcomes. Patient-derived tumor organoids (PDTOs) model tumor behavior across an array of malignancies. We leverage PDTOs to characterize the landscape of drug resistance and sensitivity in sarcoma, collecting 194 specimens from 126 patients spanning 24 distinct sarcoma subtypes. Our high-throughput organoid screening pipeline tested single agents and combinations, with results available within a week from surgery. Drug sensitivity correlated with clinical features such as tumor subtype, treatment history, and disease trajectory. PDTO screening can facilitate optimal drug selection and mirror patient outcomes in sarcoma. We could identify at least one FDA-approved or NCCN-recommended effective regimen for 59% of the specimens, demonstrating the potential of our pipeline to provide actionable treatment information.

INTRODUCTION

Sarcomas are a family of rare and heterogeneous tumors of mesenchymal origin.[1] They primarily arise in bone and soft tissue and disproportionately impact young patients.[1–3] Despite a low incidence, with ~13,000 soft tissue sarcoma and ~4,000 bone sarcoma annual diagnoses in the United States,[3] fatalities remain high. Bone sarcomas, for instance, are the third leading cause of cancer deaths in patients under 20 years old.[3] The treatment regimens vary greatly by disease subtype and stage, and therapeutic options include surgical resection, chemotherapy, targeted systemic therapy, and radiotherapy in certain cases.[4,5] Despite significant advances for specific subtypes, current treatment approaches are rarely curative and contribute to aggregate overall 5-year survival rates of ~65% in soft tissue sarcoma and ~50%–60% for bone cancers.[6]

The heterogeneity of sarcoma manifests in over 100 distinct subtypes. Diversity is observed across and within sarcoma diagnoses: for instance, there are 9 distinct osteosarcoma subtypes reported.[7] About a third of sarcomas are driven by specific chromosomal fusions, such as Ewing sarcoma, synovial sarcoma, infantile fibrosarcoma, and rhabdomyosarcoma (RMS).[8] Other key genetic events across bone and soft tissue sarcomas are thought to impact cell cycle regulation, growth factor signaling, and angiogenesis.[9] Specific high-prevalence alterations include receptor tyrosine kinase (RTK) driver mutations among gastrointestinal stromal tumors (GIST),[10] cyclin-dependent kinase (CDK) aberrations in liposarcomas,[10] and phosphatidylinositol 3-kinase (PI3K) pathway alterations in perivascular epithelioid cell tumors (PEComas) and myxoid liposarcomas.[10] Other tumor types, such as osteosarcoma and undifferentiated sarcomas, are complex karyotype tumors that can carry multiple alterations and do not have a single, well-defined driver.[11,12] This vast heterogeneity compounds the challenge to identify effective regimens for this family of rare and ultra-rare cancers and contributes to persistently low survival rates.

Precision medicine approaches are attracting increasing interest as tools to identify actionable characteristics and improve outcomes on a per-patient basis.[13] Technologies such as next-generation sequencing (NGS) and immunohistochemistry are widely used to identify molecular alterations and druggable targets.[13–16] In the case of fusion-positive sarcoma, most of the aberrant oncogenes cannot be targeted directly, with the notable exception of neurotrophic tyrosine receptor kinase (NTRK).[8] A recent study on over 7,400 bone and soft tissue sarcomas found an average of ~32% of tumors harboring actionable alterations by NGS.[17] Despite this, few sarcoma patients show clinical benefit when treated with drugs selected via genomic precision medicine, as demonstrated in many clinical trials over the past 10 years.[9,13,18,19]

Because of this genetic diversity and the limited efficacy of chemotherapeutic and targeted agents selected through both conventional or precision medicine, there is a critical need to identify alternative approaches to systematically evaluate the landscape of drug sensitivity and resistance in sarcoma and pinpoint individualized therapeutic solutions. Here, we leverage patient-derived tumor organoid (PDTO)-based functional assays as an alternative, yet complementary, approach to genetic-based precision medicine in sarcoma.[20] Patient-derived tumor organoids (PDTOs) are ideally suited to fill this gap, as they are tractable and predictive of response to treatment, at least for patients with various types of epithelial cancers.[21–28] The development of sarcoma PDTOs has lagged, with limited applications so far.[29–31]

We have procured n = 194 specimens from 126 patients undergoing biopsies or surgical resections at UCLA Health hospitals and successfully generated PDTOs from over 110 samples originating from primary, recurrent, and metastatic bone and soft tissue sarcomas. Here we describe our pipeline for procuring and generating sarcoma PDTOs, which includes histopathology to characterize both the parent tumor and PDTOs as well as sequencing and high-throughput drug testing leveraging our rapid three-dimensional (3D) organoid screening platform.[20,29,32–34] The drug sensitivity and resistance patterns observed across 24 sarcoma types highlighted both subtype-specific and patient-specific vulnerabilities.

RESULTS

Establishment and characterization of soft tissue and bone sarcoma PDTOs

We collected a total of n = 194 sarcoma specimens from 126 patients treated at UCLA for a sarcoma diagnosis between February 2018 and May 2022 (Figure 1). Patient features and sample types are shown in Figures 1 and S1 and described in the STAR Methods section. The specimens included in this study were procured through the UCLA Pathology Department and expedited to the lab for processing (Figure 1A).[20,29,32–34] Given that there is no a priori sorting of tumor cells, we performed a detailed histopathological analysis of organoids and parental tissue to verify that tumor cells were present and all main features were maintained *ex vivo*[29,32] (Figure 2A). We observed diverse histopathological features across sarcoma subtypes, such as small round blue cells in Ewing sarcoma, vacuolated cells with round nuclei in chordoma, and spindle cells in RMS, some types of osteosarcomas, and malignant peripheral nerve sheath tumors (MPNSTs), characteristics that were recapitulated in organoids (Figures 2A and S2A).

We employed serial bright-field imaging to quantitatively assess the growth of organoids *ex vivo*[29] (Figure 2A). Plates were imaged once every 24 h and growth rates quantified by applying a U-net machine learning-based segmentation algorithm that quantifies the cross-sectional area occupied by organoids[29,35] (Figure 2A). Organoids derived from undifferentiated pleomorphic sarcoma (UPS), leiomyosarcoma (LMS), and chordoma demonstrated minimal increases in normalized area over 5 days. This aligns with our previous findings in chordoma organoids, where limited proliferation and cell rearrangement were observed in PDTOs from multiple patients.[29] By contrast, PDTOs from patients diagnosed with myxofibrosarcoma, RMS, epithelioid sarcoma, and Capicua transcriptional repressor (CIC)-rearranged sarcoma exhibited exponential growth, characterized by cell aggregation and proliferation, leading to extensive networks of multicellular clusters with large cross-sectional areas (Figure 2A).

We confirmed that key sarcoma drivers and molecular features are preserved within the PDTOs. For example, most well-differentiated liposarcomas, like SARC0120, show mouse double minute 2 homolog (MDM2) amplification, a hallmark of this cancer. Diagnostic fluorescence *in situ* hybridization (FISH) on the parental tumor confirmed MDM2 amplification (Figure S2B), and FISH analysis of SARC0120 organoids also showed this alteration, consistent with the original tumor (Figure S2C). RNA sequencing (RNA-seq) analysis showed that molecular features were consistent between genomically diverse sarcomas and their respective organoids (Figures 2B and 2C), with Spearman's rank coefficients consistently above 0.8 for 32 organoid and primary tumor pairs (median = 0.87, Figures 2B and S2D). Our data shows that PDTOs from various sarcoma subtypes preserve the key histological and molecular features of the original tumor while displaying diverse *ex vivo* growth dynamics. This indicates that PDTOs retain both subtype-specific and patient-specific sarcoma phenotypes within our standardized organoid culture approach.

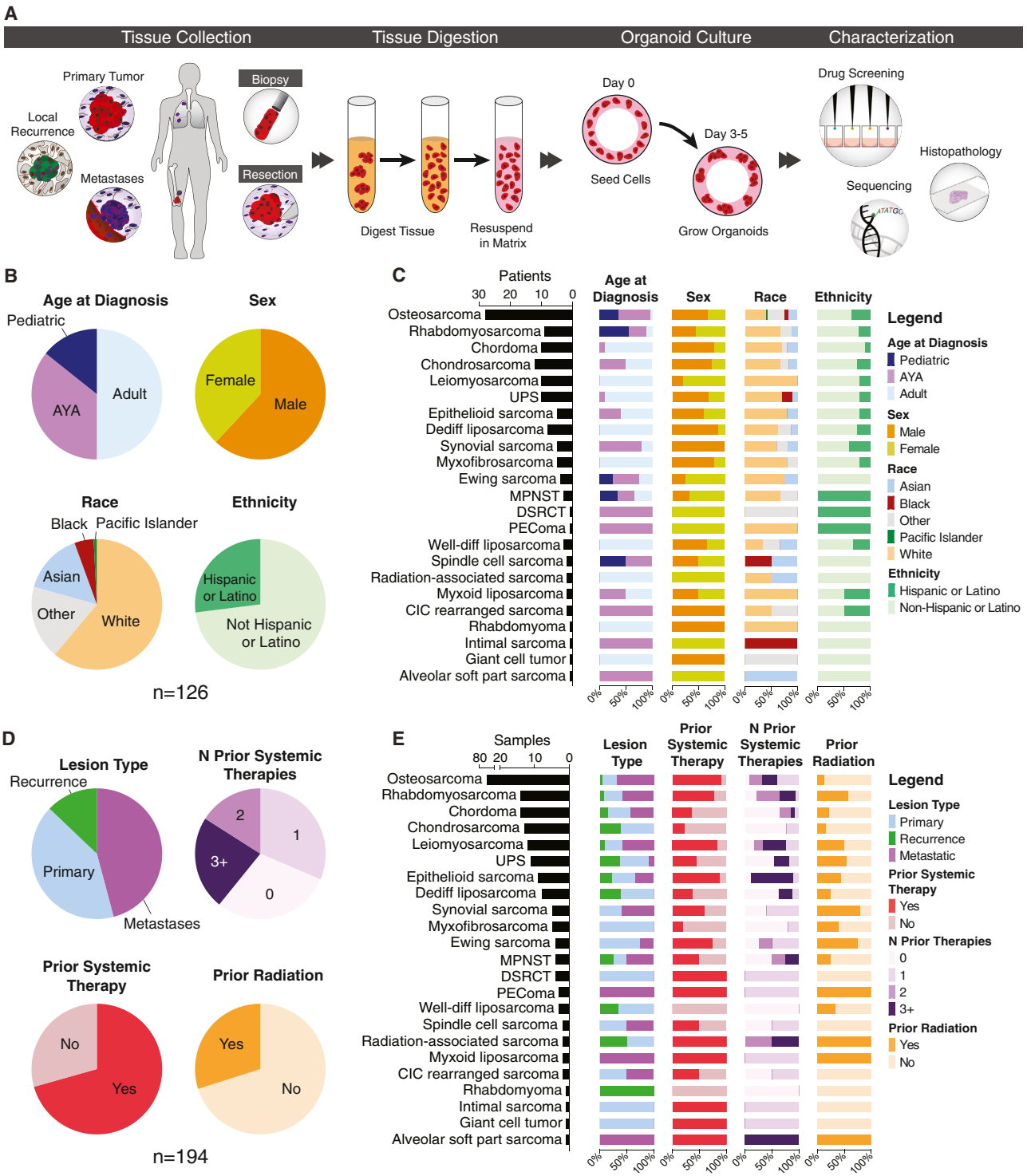

Figure 1. Overview of the patient-derived tumor organoid pipeline, patient demographics, and sample characteristics

(A) Tissue is collected from biopsies or surgical resections of bone and soft tissue sarcomas. Organoids are generated by digesting the tissue and culturing the harvested cells in a 3D matrix. Organoids are molecularly and functionally profiled.

(B) Demographics of pan-sarcoma study patients. Pediatric: 0–14 years old, AYA: 15–39 years old, and adults: 40 years old and above.

(C) Demographics divided by diagnosis.

(D) Clinical characteristics of tumors from which tissue was collected. Prior systemic therapies include chemotherapy, targeted agents, and immunotherapy.

(E) Tumor characteristics divided by disease subtype.

See also Figure S1.

CellPress
OPEN ACCESS

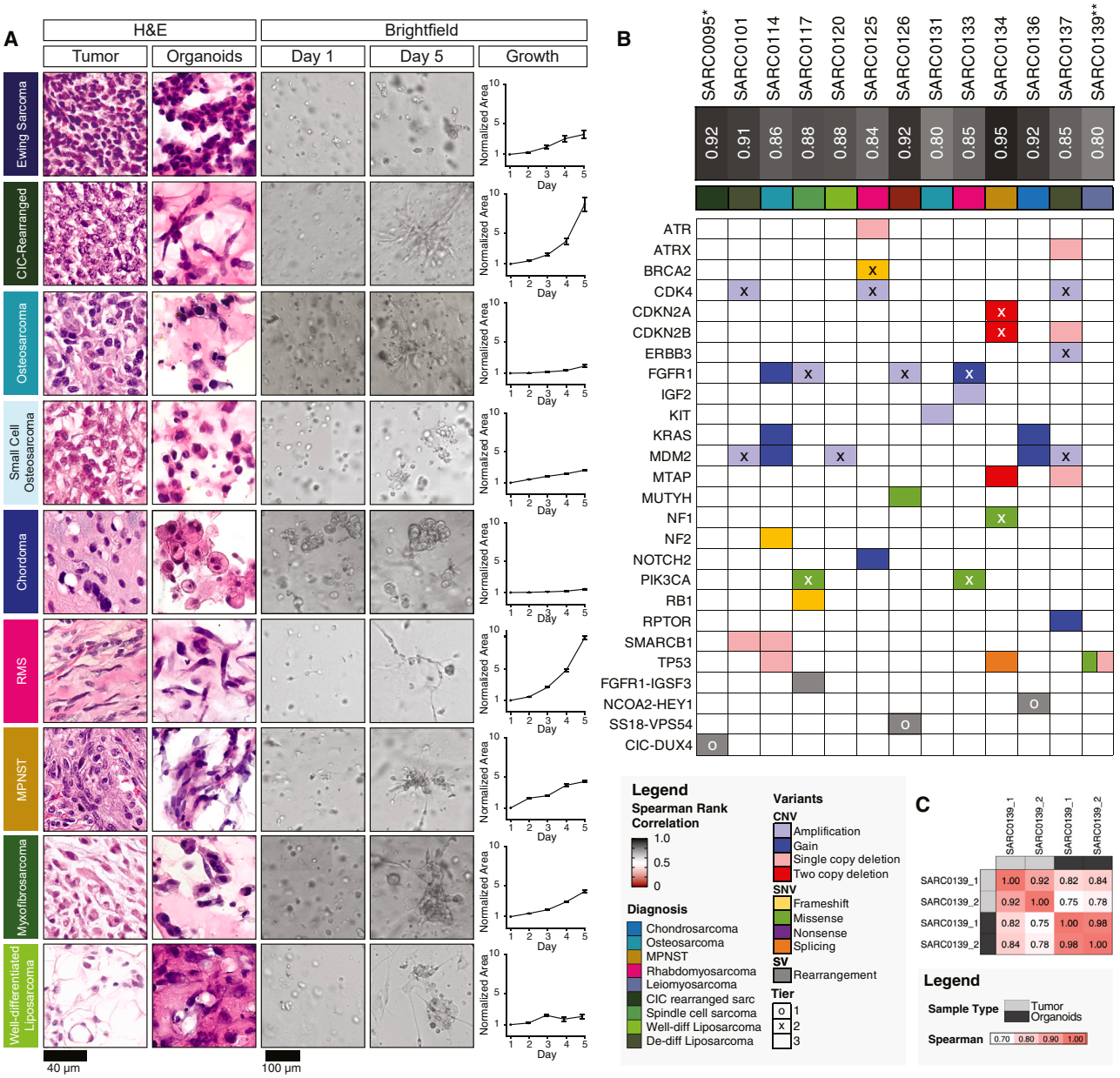

Figure 2. Sarcoma organoids grow in culture and recapitulate key morphological features of the parental tumors

(A) Representative images of sarcomas and corresponding organoids stained with H&E (columns 1 and 2). Representative bright-field images of the same sarcoma cells in culture on day 1 (column 3) and day 5 (column 4). Growth was tracked over time by segmenting in-focus organoids in the bright-field images using a machine learning-based pipeline and by normalizing the cross-sectional area covered by organoids to that measured on day 1 of culture. Data are represented as mean ± SEM. Scale bars: 40 μM for H&E images and 100 μM for bright-field pictures.

(B) Genomic and transcriptomic characterization of selected sarcoma samples. Dark boxes below sample names are Spearman's rank correlation coefficients comparing the frequency of RNA transcripts across RNA-sequenced tumor and organoid samples. Correlations exclude genes with expression less than 0.1 transcripts per million in either sample. The table below shows findings from genomic characterization of tumor samples with the Dana-Farber Cancer Institute OncoPanel version 3.1. Colors in the heatmap indicate the type of the copy number variant (CNV), single-nucleotide variant (SNV), or structural variant (SV). Tier, indicated by an "o" or "x" superimposed on the plot, represents the classification scale. Tier 1 represents alterations with "well-established published evidence" of diagnostic or prognostic value, tier 2 alterations "may have clinical utility," and tier 3 alterations have "uncertain clinical utility."

(C) Spearman's rank correlation coefficients comparing RNA transcripts of tumor and organoids derived from two samples collected from patient SARC0139. Genes with expression less than 0.1 transcripts per million are excluded from the analysis.

See also Figure S2.

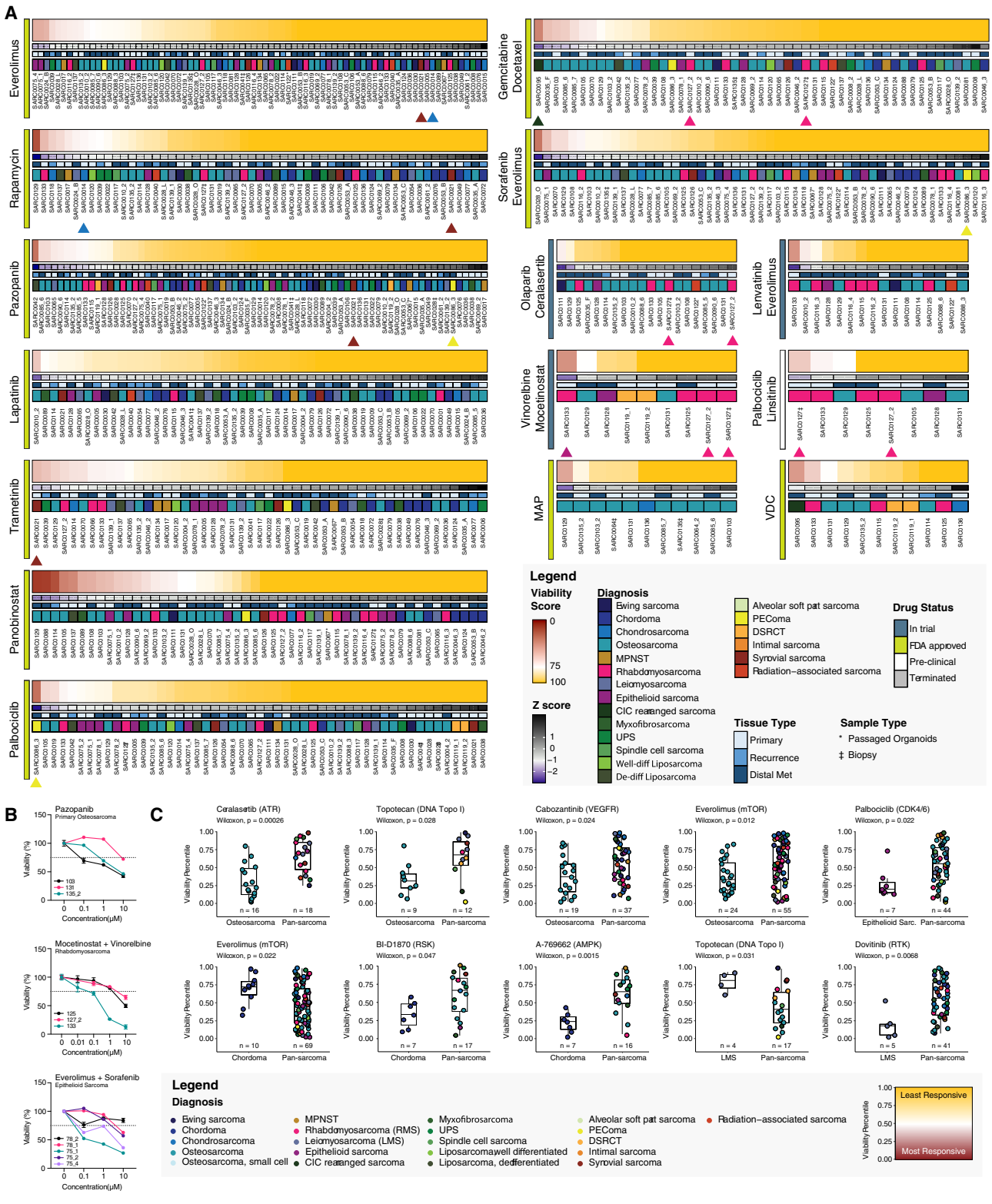

Figure 3. Sarcoma organoid sensitivity to treatment in high-throughput drug screening experiments shows a range of responses

(A) Heatmaps of organoid sensitivity to selected drugs of interest at 1 μM. The viability score represents each organoid model's viability normalized to the mean response to treatment across all samples. Each column is a unique specimen, red indicates higher sensitivity to treatment than average. Colored bars underneath each heatmap represent the *Z* score, lesion type, and diagnosis of each sample. * indicates passaged samples and ‡ denotes biopsies. Samples with the same SARC number are derived from the same patient.

(legend continued on next page)

Sarcoma PDTO screening pipeline

We procured n = 194 samples, which were expedited to the lab for downstream characterization and screening (Figure S3A). Multiple samples were collected from 27 patients. Of all collected samples, 21 had insufficient cell number for further analyses, with fewer than 250,000 viable cells recovered. Four additional samples had low cell numbers but were seeded for expansion and passaging yet failed to grow. Lastly, two samples were excluded due to contamination by ink marking during the pathology workflow, and three were used for other studies. 40 samples were frozen, including 19 that were procured during COVID-related shutdowns and interruptions. The remaining 124 samples (80% of all processed) encompassing 21 different sarcoma diagnoses were used to generate mini-rings[20,29,32–34] in 96 well plates for high-throughput screening. Ten samples showed no growth, resulting in an organoid take rate of ~93% for all samples we attempted to screen or grow and expand (Figure S3A).

We assessed drug screening quality using Z' factor and robust Z',[36,37] including plates with Z' or robust Z' factor $\geq$0.2 in downstream analyses (Figures S3B and S3C). Our drug library comprised over 400 compounds and combinations at various clinical and pre-clinical development stages (Figures 3A and 3B).[29,32,34] Drug screening panels were tailored to each sample based on individual characteristics, histology, patient data, and clinical background, focusing on FDA-approved therapies, National Comprehensive Cancer Network (NCCN)-recommended regimens, and drugs targeting genetic alterations identified in the samples. Where feasible, we also considered the anticipated clinical treatment plan. The number of drugs tested per sample varied, averaging 117 (range: 6–423), depending on the number of extracted cells and the specific drug panel. This customized approach enabled a thorough assessment of treatment options, uniquely tailored to each sample's clinical and molecular profile.

The landscape of drug sensitivity and resistance in sarcoma PDTOs

Sarcoma PDTOs were tested against chemotherapy or targeted drugs as single agents or in combination. We included approved therapies used in sarcoma such as sorafenib and everolimus, gemcitabine and docetaxel, and methotrexate, doxorubicin, and cisplatin (MAP,[4,5] Figures 3A, 3B, and S4A). To account for variations in drug efficacy, such as in the case of broadly cytotoxic molecules,[38] we calculated a viability score by normalizing the viability of each specimen to the average measured across all samples treated with the same regimen (Figure 3A). By employing this approach, we identified individual samples that displayed unique sensitivities to specific therapies, with a subset of single and combinatorial regimens shown in Figure 3.

Among the 92 specimens screened against 10 or more compounds included in our analysis, the majority (74/92, 80.4%) had at least one significant response, defined as ranking in the top 5% of viability scores for one or more tested regimens. Three samples (3.3%) showed this high level of sensitivity to a quarter or more of the compounds tested, suggestive of a broad and possibly nonspecific chemosensitivity. By contrast, 18 sarcomas (19.6%) did not achieve top 5% rankings for any compound. These samples were typically tested against smaller drug libraries, averaging 54 regimens per sample, compared with 116 for those with at least one significant response (median: 25 vs. 58 drugs or combinations), which indicates how smaller screens may be insufficient to identify effective regimens. Samples generally showed specific responses: SARC0021, a synovial sarcoma, was highly sensitive to the mitogen-activated protein kinase kinase (MEK) inhibitor trametinib[39] (viability score: 54), but among the most resistant to pazopanib, palbociclib, rapamycin, and everolimus (Figure 3A, brown arrowhead). PDTOs from SARC0086_3 PEComa had the highest sensitivity to palbociclib but were strongly resistant to pazopanib and the sorafenib-everolimus combination (Figure 3A, yellow arrowhead).

We observed varied sensitivities to compound classes, such as among the 56 samples screened against mTOR inhibitors everolimus and rapamycin. Of these, 14% were responsive to both drugs, ranking in the top quartile of responders. Notably, PDTOs from the de-differentiated chondrosarcoma SARC0014 were highly sensitive to rapamycin (top quartile) but resistant to everolimus (bottom quartile, Figure 3A, blue arrowhead). Bone tumors like chondrosarcoma and chordoma are considered broadly chemoresistant.[29,40,41] This aligns with our data, where these tumor types frequently show resistance to therapy, as seen in the low response rates to everolimus for chordoma and chondrosarcoma PDTOs, which account for 4 of the 5 most resistant samples (Figure 3A).

We explored the effectiveness of combination therapies, including those in clinical use or trials (Figures 3A and 3B). SARC0095, a CIC-rearranged sarcoma, showed remarkable sensitivity to gemcitabine and docetaxel (viability score: 36, green arrowhead). Gemcitabine-based regimens have been reported to induce two partial responses in CIC-rearranged sarcomas.[42] The combination of vinorelbine and mocetinostat is currently in trials for RMS.[43] We observed an exceptional response for the RMS SARC0133 (Figure 3A, magenta arrowhead), with heightened sensitivity across all tested concentrations when compared with other three RMS samples (Figure 3B). In summary, the drug sensitivity profiles across a broad spectrum of sarcomas revealed distinct response patterns, highlighting the approach's utility in identifying unique resistant and responsive cases for personalized strategies.

Intra-patient tumor heterogeneity in drug sensitivity

We obtained multiple lesions for 21% of patients and calculated Pearson correlation coefficients for cases with at least two screened samples, considering all overlapping drugs at every concentration (Table S1). Notably, we observed both

(B) Dose-response curves of organoid viability when treated with selected therapeutic regimens. Percent viability is reported compared with vehicle-treated organoids for each individual sample. Data are represented as mean ± SEM.

(C) Sensitivity rank plots comparing the response of organoids derived from the indicated diagnoses (left) against pan-sarcoma specimens (right). Samples are ranked from low residual viability percentile (most responsive samples) to the highest residual viability percentile (least responsive samples). Primary drug targets are indicated next to each drug's name. The color of each point represents the diagnosis of the individual samples. Boxplots represent the interquartile range. See also Figures S3 and S4 and Table S1.

concordant and discordant responses, even for samples from the same surgery. We compared three metastatic lesions from an epithelioid sarcoma with undifferentiated pleomorphic features, SARC0075, procured during the same surgery. SARC0075_1 and 4 responded to ~23% of the tested drugs and were closely correlated (Pearson coefficient 0.84). However, a third lesion, SARC0075_2, had a different profile, responding to only 7.7% of regimens and showing marked resistance to everolimus across all doses (Figure 3A). Sample 2 was the least similar to the other metastases, with Pearson coefficients of 0.64 and 0.66 compared with samples 1 and 4. This mirrors the clinical heterogeneity observed in the patient, including varied tumor-to-tumor responses to treatments like temozolomide, highlighting how the behavior measured *ex vivo* can capture biological features of clinical relevance. Conversely, SARC0139_1 and 2, two LMS metastases from a single procedure, showed strong correlation (Pearson 0.8), consistent with their transcriptome similarity (Figure 2C; Table S1).

We had three cases of repeat PDTOs from a biopsy and subsequent tumor resection: two osteosarcomas and a therapy-naive RMS. The RMS, SARC0127, was biopsied shortly before surgery (18 days) and received no therapy in between. Despite the brief interval between biopsy and resection, we observed some distinct differences in sensitivities, including to palbociclib/linsitinib (Figure 3A, pink arrowhead), yielding an overall Pearson coefficient of correlation of 0.87. Given the short time and lack of neo-adjuvant treatment, the heterogeneity could be related to intra-tumoral variability and sampling bias.[28] In summary, our pipeline can quantify similarities and differences in drug response within individual patients, emphasizing the importance of considering intra-patient (tumor-to-tumor) as well as intra-tumoral heterogeneity with any approach using limited tissue sampling for selecting therapeutic strategies.

Sarcoma PDTOs demonstrate subtype-specific responses to treatment

Despite the expected heterogeneity in responses among patients with the same sarcoma diagnosis (Figures 3A and 3B), we identified some disease-specific trends. We compared the viability scores for each diagnosis against all other sarcoma types using the Wilcoxon rank sum test with Bonferroni adjustment for multiple comparisons correction (Figures 3C, S4B, and S4C). We found osteosarcoma organoids to be significantly more sensitive than the pan-sarcoma average to the drugs ceralasertib, topotecan, cabozantanib, and everolimus, with p values of 0.00026, 0.028, 0.024, and 0.012, respectively (Figure 3C). Celarasertib is an ataxia telangiectasia and Rad3-related (ATR) inhibitor currently in trial in combination with olaparib for osteosarcoma.[44]

In accordance with their well-documented chemoresistance to treatment,[45,46] chordomas were significantly less sensitive than the pan-sarcoma average to everolimus (p = 0.022), alvocidib (p = 0.00046), apitolisib (p = 0.0071), and bortezomib (p = 0.000018, Figures 3C and S4C). Yet, we identified 3/256 drugs for which chordoma PDTOs established from more than two patients showed greater sensitivity than the broader population: an EGFR/HER2 kinase inhibitor, TAK-285 (p = 0.034), which also targets Aurora B and MEK; a ribosomal S6 kinase (RSK) inhibitor, BI-D1870 (p = 0.047); and an AMP-activated protein kinase (AMPK) activator, A-769662 (p = 0.0015, Figure 3C). RSK links MAPK/ERK signaling to the regulation of AMPK activity through LKB1. RSK inhibition results in AMPK activation,[47] thus the BI-D1870 and A-769662 compounds have overlapping biological effects. Our findings support interrogating this pathway further in the context of chordoma.

We observed a number of other trends in cohorts with smaller sample sizes, such as chondrosarcoma PDTOs sensitivity to the FAK/Pyk2 inhibitor, TAE226 (p = 0.04), and to the PDK1 inhibitor, BX-912 (p = 0.038), RMS organoids to pazopanib (p = 0.049), and trametinib (p = 0.013), and UPS organoids to the insulin growth factor (IGF)-1R inhibitor, BMS-754807 (p = 0.039, Figure S4B). Lastly, LMS organoids exhibited lower responses to topotecan (p = 0.031, Figure 3C) than other sarcomas, consistent with previous clinical trials indicating that topotecan is ineffective in LMSs.[48] The replication of known response patterns *ex vivo* is crucial for validating novel findings. For example, LMS was significantly more sensitive than other sarcomas to the broadly active kinase inhibitor dovitinib (p = 0.0068), a drug not currently under investigation for this disease. These trends may aid in the identification of new indications for therapeutic regimens.

Clinical features associated with drug responses

We performed the same analysis described above to identify other correlates of response, including clinical features such as patient age at diagnosis, lesion type (primary, metastatic, or recurrent disease), treatment history, and disease progression (Figure 4). We identified trends on small numbers of compounds yielding differences in viability scores for tumors exhibiting certain characteristics. For instance, tumors exposed to prior systemic therapies of any kind up to 3 months prior to tissue procurement appeared slightly more sensitive than treatment-naive sarcomas to molecules such as the mTOR inhibitor everolimus or the multi-tyrosine kinase inhibitors (TKIs) cabozantinib, lenvatinib, and cediranib (p = 0.018, p = 0.036, p = 0.011, and p = 0.017, respectively; Figures 4 and S4D) yet more resistant to golvatinib (p = 0.036, Figure S4D). Stratification by number of previous therapies (0 vs. 1−2 vs. 3+) highlighted that tumors exposed to more (3+) drugs were more sensitive than naive ones to pazopanib, BI2536, and danusertib (p = 0.0062, p = 0.046, and p = 0.011, respectively), or PHA−767491 and lenvatinib for sarcomas treated with one or two lines of systemic therapy (p = 0.029 and p = 0.035, respectively, Figures 4 and S4D).

Patient age correlated with patterns of response; for instance, sarcoma PDTOs derived from adults showed greater resistance to cediranib compared with both pediatric (p = 0.032) and adolescent and young adult (AYA) (p = 0.013) sarcomas. PDTOs from adults were more sensitive than AYA to the Janus kinase (JAK) inhibitor WHI-P154 (p = 0.0037) (Figure 4). Taking into account the stage of disease, metastatic sarcoma PDTOs exhibited a tendency toward enhanced responses to degrasyn when compared with primary or recurrent tumors (p = 0.028 and p = 0.048) and to OSI-930 when compared with primary tumors (p = 0.024, Figure 4). The observed differences in treatment response among various sarcomas were influenced by the age-specific prevalence of these tumors, as well as variations in disease management and treatment protocols.[49–51] Notably, cediranib is overall more effective on osteosarcomas than other

Figure 4. Sarcoma organoid sensitivity correlates with clinical attributes

Sarcoma samples are grouped by clinical features, including patient age at diagnosis, lesion type, number of prior systemic therapies, prior systemic therapy within 3 months of sample procurement, and change in disease status. All samples screened with the indicated drug are ranked from the lowest viability percentile (reduced PDO viability, higher response to drugs) to the highest viability percentile (increased PDO viability, lower response to drug) and plotted according to the rank. Primary drug targets are listed. The color of each point represents the specific diagnosis of the individual samples. Statistical significance is tested by performing a Kruskal-Wallis test with post-hoc Wilcoxon rank sum test for pairwise comparisons with Bonferroni correction for comparisons across three classifications. For comparisons across two categories, a Wilcoxon rank sum test was performed. Boxplots represent the interquartile range.
See also Figure S4.

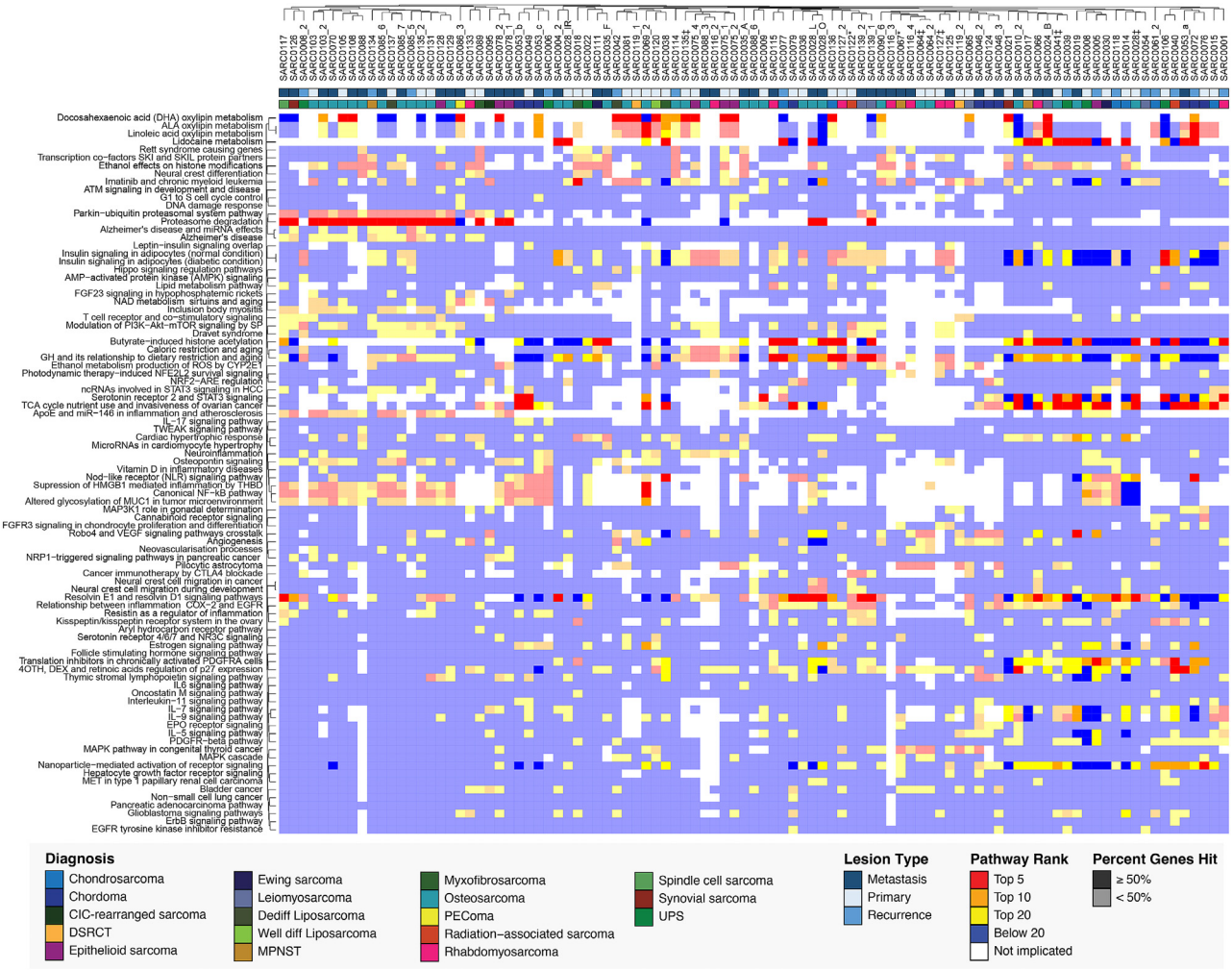

Figure 5. Landscape drug sensitivity patterns reveal vulnerable biological pathways

Heatmap showing the molecular pathways most sensitive to drug targeting for each screened sample from WikiPathways. Similar pathways are clustered together using the Jaccard distance, and samples are clustered together by their Euclidian distance. Pathways are ranked independently for each sample based upon the results of drug screening experiments. Pathways targeted by the most effective drugs are ranked highest (red). Opaque squares indicate pathways in which more than 50% of the constituent genes were targeted in the drug panel. Pathways ranked in the top 50 for 20 or more samples are plotted. White squares indicate that the pathway was not targeted by any drugs in the screening experiments.

See also Figure S5.

histologies (Figure S4D); thus, it is not surprising that pediatric and AYA sarcoma PDTOs were more sensitive than adults, given the prevalence of osteosarcoma in our pediatric and AYA cohorts (Figure 4). Similarly, a large portion of metastatic samples in our dataset are osteosarcomas (17/40, 42%), while the chemoresistant chordomas are overrepresented among primary tumors (4/42, 10%). Therefore, while the trends reported are significant, they are strongly associated to specific sarcoma subtype characteristics.

Lastly, we investigated organoid response patterns with respect to changes in disease trajectory at time of follow-up. A change in status was defined as either a tumor recurrence following resection or the identification of metastatic disease from previously primary or localized recurrent tumors. PDTOs derived from patients who developed progressive disease were significantly more resistant to treatment with dasatinib ($p = 0.039$), rapamycin ($p = 0.014$), and gefitinib ($p = 0.048$, Figures 4 and S4). Tumors that rapidly progressed had increased sensitivity to thiazovivin, a ROCK inhibitor, as well as sorafenib and ruxolitinib ($p = 0.041$, $p = 0.042$, and $p = 0.043$, respectively; Figures 4 and S4).

Target analysis of drug responses highlights vulnerable biological pathways in sarcoma

We conducted a comprehensive analysis of drug sensitivity profiles in sarcoma organoids to identify the molecular pathways contributing to drug responses[29] (Figures 5 and S5A). We mapped each drug to their gene targets and pathways using the PubChem and WikiPathways[52] (Figure 5) or KEGG pathways[53] (Figure S5A) databases. We then ranked the pathways from most impactful (Figure 5, red) to least impactful (Figure 5, blue) on the basis of their weighted components' contribution to

CellPress
OPEN ACCESS

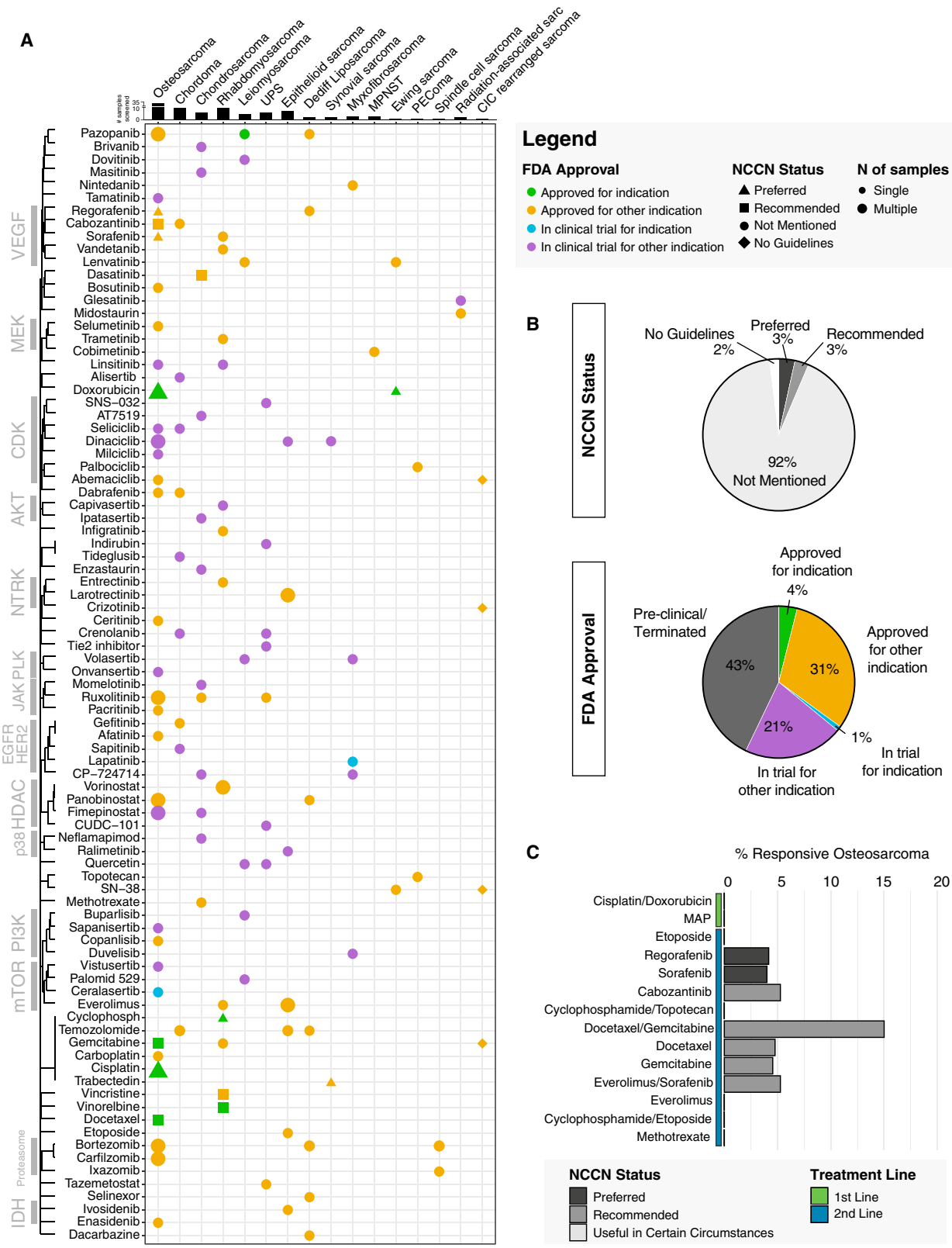

Figure 6. Actionability of PDTO predictions determined by drug approval status

We selected drug-diagnosis pairs of interest by cross-referencing the five most effective drugs for each sample with the 10% most responsive samples for each drug.

(legend continued on next page)

reduction in organoid viability scores (Figure 5). Interestingly, despite variations observed during the analysis of individual drugs (Figures 3; Table S1), we consistently observed a tendency for samples derived from the same patient to cluster together. This pattern held true for SARC0103, SARC0078, SARC0075, SARC0139, and SARC0053, suggesting that sarcomas originating from the same patient share overarching vulnerabilities in molecular pathways, regardless of differences in tumor type, tumor location, timing of surgery, or response to specific drugs.

Sarcoma samples by and large did not cluster by histology, with some exceptions, highlighting the individual heterogeneity within sarcoma subtypes (Figure 5). For instance, organoids derived from chordoma patients SARC0053 and SARC0049 clustered together due to sensitivity to treatments targeting genes in the serotonin receptor 2 and STAT3 signaling pathways as well as genes associated with TCA cycle (Figure 5), confirming our previous analysis.[29] These pathways contributed to the observed responses for a second group of samples encompassing both bone and soft tissue sarcomas (Figure 5). Perturbations in blood vessel-related pathways such as angiogenesis, Robo4, and vascular endothelial growth factor (VEGF) signaling were linked to responses in a group of samples, which included chordoma, desmoplastic small round cell tumor (DSRCT), and LMS cases (Figure 5). Additionally, we found a cluster of 9 samples with vulnerabilities in the oxylipin metabolism pathway and, partially, in the insulin signaling pathway (Figure 5). Oxylipin derivatives have been linked to cancer cell proliferation.[54] Inflammation-related pathways were ranked as highly impactful across a broader set of 17 samples originated from a variety of histological subtypes (Figure 5).

The same analysis performed using the KEGG database allowed us to identify additional groups of pathways. For instance, EGFR and ErbB signaling pathways were significantly implicated in sensitivities observed in a group of samples that included chordomas (SARC0046_2 and 3, SARC0053_a, and SARC 0049; Figure S5A), a subgroup of osteosarcoma samples (SARC0019, SARC0036, SARC0010_2, and SARC0041; Figure S5A), and soft tissue sarcomas such as LMS and RMS (SARC0065 and SARC0127_2, respectively; Figure S5A). Overall, this pathway analysis shows how PDTOs capture patient-specific features and susceptibilities yet often transcend the histological subtype that currently dictates their treatment.

Clinical availability of PDTO-selected drugs: A roadmap to actionability

As there is increasing interest in leveraging PDTOs for precision medicine, we set to determine the degree of actionability of the drug sensitivities identified with our approach.[29,38,55] We define a drug or combination as actionable if it could be prescribed on- or off-label or accessed in the context of a clinical trial. To quantify actionability within our dataset, we generated a ranked list of the top 5 most effective regimens for each sample using the viability scores of single drugs and combinatorial treatments. We further refined the list by only including regimens in downstream analysis if the patient ranked within the top 10% of responders. This allowed us to eliminate generally ineffective drugs for highly chemoresistant samples. We then annotated the identified drugs by FDA status and recommendation on the basis of NCCN[4,5] Guidelines, if any (Figure 6).

After aggregating drugs by diagnosis, we identified $n = 203$ drug-diagnosis pairs, that is, molecules found as effective in at least one patient with a certain subtype of sarcoma. This pairing allows us to verify approval status for specific indications (Figures 6A, S5B, and S5C). Of these 203, 4% are FDA-approved for the same sarcoma type that was found as *sensitive ex vivo*, while 31% are approved for other cancers (Figure 6B). Given the rarity of sarcomas as a whole and limited number of existing trials, only 1% of the drugs identified are in clinical trials for the organoid-directed indication, while 21% are in trials for other cancers (Figure 6B). Finally, 43% of the identified compounds are unavailable clinically either because they are in pre-clinical development or terminated (Figure S5B), whether it be because of limited efficacy in an unstratified population, toxicities, or other factors.[56] Our analysis also identified $n = 24$ combinatorial regimens fulfilling the criteria above (Figure S5C).

We next took into account NCCN Guidelines for patients with bone[5] and soft tissue[4] sarcoma. The inclusion of a therapeutic regimen in these clinical guidelines requires substantial evidence of both safety and efficacy. Due to the small patient populations and highly heterogeneous disease, the vast majority (92%) of drug regimens we identified are not incorporated in current guidelines. Only 5% of these are listed as preferred regimens by the NCCN for their corresponding histological subtype, such as etoposide, cisplatin, sorafenib, and regorafenib for osteosarcoma, cyclophosphamide for RMS, and doxorubicin for osteosarcoma and Ewing sarcoma (Figure 6A). An additional 3% of drugs are recommended for their respective diagnosis, including cabozantinib, gemcitabine, docetaxel, and everolimus for osteosarcoma and doxorubicin and vinorelbine for RMS (Figure 6A). The remaining 93% of drugs are beyond the recommendations of the NCCN Guidelines, either not mentioned (90%) or no guideline is available yet for the disease, as is the case for DSRCT and CIC-rearranged sarcomas.

Osteosarcoma has well-established NCCN[5] guidelines for both first- and second-line therapy (Figures 6C and S6A; Table S2). We categorized drugs used in first- or second-line therapy according to NCCN Guidelines (preferred, recommended, or useful in

(A) Current FDA-approval status and NCCN Guidelines recommendations are shown for each unique drug-diagnosis combination. Green and yellow colors indicate FDA-approved drugs for the same cancer type or for other cancer indications, respectively. Blue and purple represent drugs in trial for the same cancer or different cancers, respectively. The shape of the symbols indicates NCCN Guideline status. Triangles show drugs that are preferred and squares recommended as per NCCN Guidelines. Circles are drugs not currently discussed in the guidelines.[4,5] Diamond shape signifies that the histologic subtype has no guidelines as of yet, such as in the case of DSRCT and CIC-rearranged sarcoma. The size of the marker represents the number of samples for which each regimen is found among the most effective. Drugs are clustered by similarity in gene targets using Jaccard distance. The number of samples screened for each histologic subtype is shown in the bar charts above the graph. Cyclophosp indicates cyclophosphamide.
(B) Pie charts summarize the overall percentage of drugs that fall into each category for FDA approval and NCCN recommendations.
(C) Percentage of responsive osteosarcoma PDOs to NCCN-recommended treatment regimens.
See also Figures S5 and S6 and Tables S2 and S3.

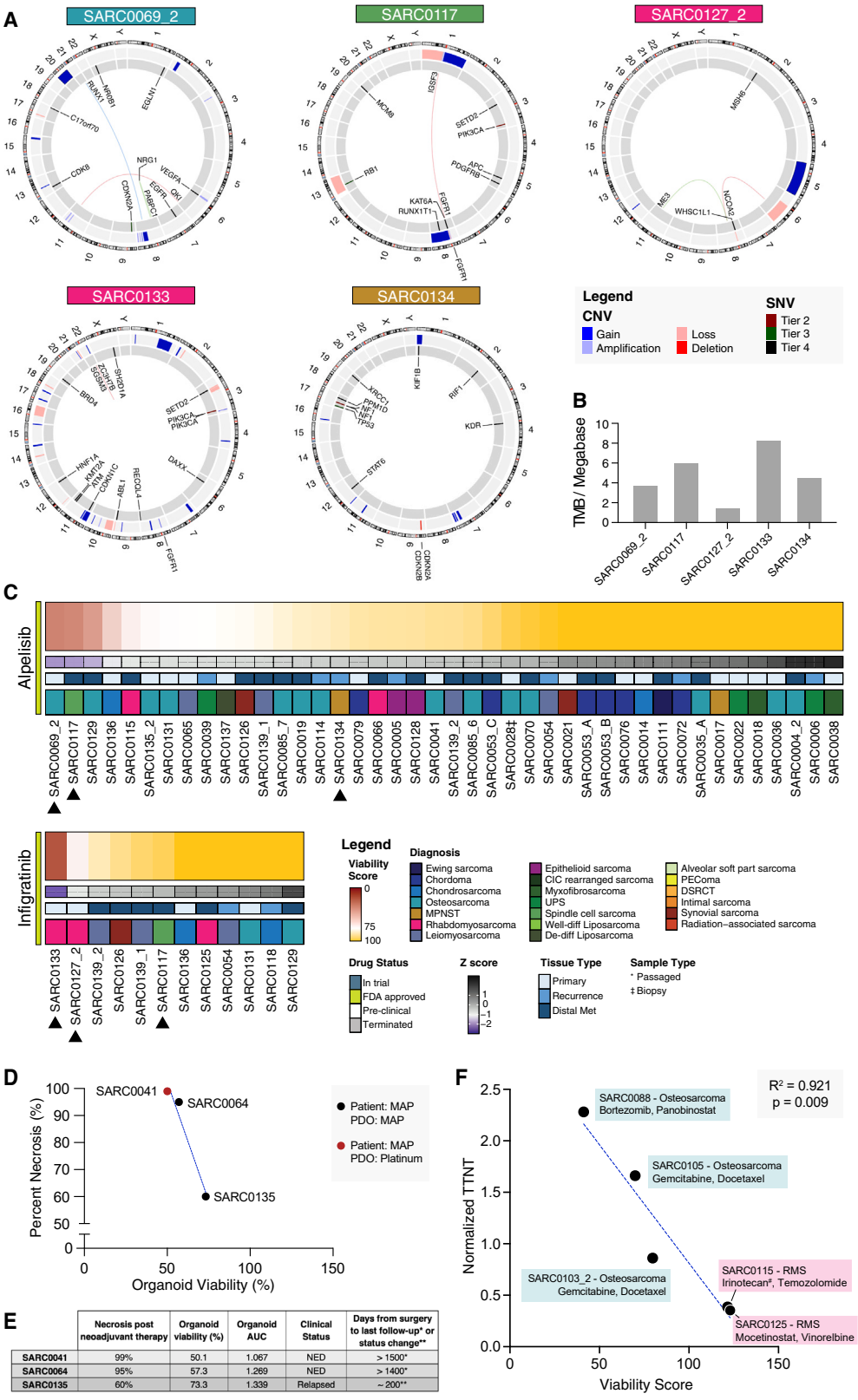

E

	Necrosis post neoadjuvant therapy	Organoid viability (%)	Organoid AUC	Clinical Status	Days from surgery to last follow-up* or status change**
SARC0041	99%	50.1	1.067	NED	> 1500*
SARC0064	95%	57.3	1.269	NED	> 1400*
SARC0135	60%	73.3	1.339	Relapsed	~ 200**

Figure 7. Organoids provide genomic and diagnostic information

(A) Summary of the genetic features of selected sarcomas. Sequencing was performed using OncoPanel.

(B) Tumor mutational burden (TMB) for the same samples.

(legend continued on next page)

certain circumstances, Figure 6C; Table S2). Osteosarcoma is conventionally treated with a combination of MAP in the first-line setting.[57] We observed expected sensitivities to MAP in osteosarcoma PDTOs (see Figure 7), in line with clinical experience. Yet, this regimen was not among the top 5 most effective ones in the samples tested (Figure 6C). Of the second-line regimens, the combination of gemcitabine and docetaxel produced top responses in ~15% (3/20) of the osteosarcoma PDTOs. Various second-line treatments were effective in small subsets of patients, including regorafenib (1/24), cabozantinib (1/19), docetaxel (1/21), and gemcitabine (1/22, Figure 6C; Table S2). The broad heterogeneity in responses observed clinically is mirrored in our screening results. For instance, the combination of sorafenib-everolimus was effective in ~5% (1/19) of screened osteosarcoma PDTOs, including SARC0028_O (Figure S7). Results are consistent with the clinical trial outcomes in advanced and progressing osteosarcoma, with two partial responses (per RECIST criteria)[58] and two minor responses (less than 30% and more than 10% reduction in lesion size per study criteria) recorded out of $n = 38$ patients.[59] Our findings support the notion that functional precision medicine approaches may help matching each patient to the optimal therapeutic regimens.

In aggregate, we found that the most effective drugs included at least one FDA-approved or NCCN-recommended regimen for 59% (57/97) of sarcoma samples we screened (Table S3A). Most samples had a single FDA-approved drug or NCCN-recommended regimen among the most effective ones (34/57), while 2 samples had four actionable effective drugs according to our criteria (Table S3A). When analyzing patient-level data, we identified active, approved, or recommended therapies for 58% of the patients screened (43/74). Specifically, 18 patients had one approved therapy that was considered among the most effective, while 7 patients had 4 (Table S3B). For patients from whom we collected multiple samples (12% of patients screened, 9/74), 4 patients had two approved drugs as most effective, and 5 patients had four (Table S3C).

Functional screenings provide orthogonal and complementary information to genomic sequencing

Both functional screenings and genomic sequencing can provide clues to identifying drivers of disease and therapeutic leads (Figures 7A and B). Mutations in the PIK3CA gene are linked to clinical responses to PI3K inhibitors such as alpelisib in some tumor types.[60–62] A metastatic undifferentiated spindle cell sarcoma (USS, SARC0117) carried the hotspot H1074L mutation in PIK3CA[61,63,64] and its PDTOs were among the strongest responders to alpelisib (Figure 7B). Conversely, metastatic tissue from SARC0134, an MPNST with the same H1074L mutation clinically reported in the primary tumor, showed no response (Figure 7B). Follow-up sequencing of the lesion used to establish PDTO demonstrated no PIK3CA mutation in the metastasis (Figure 7A), confirming the screening results. Interestingly, the top responder to alpelisib, SARC0069_2, is a PDTO derived from a primary osteosarcoma with no mutations in the PIK3CA gene (Figure 7A), which emphasizes how organoids can both validate sequencing and identify biomarker-negative responders.

We tested 8 mTOR/PI3K pathway inhibitors on SARC0117. This sample ranked among the top 3 most sensitive to apitolisib, alpelisib, copanlisib, BGT226, and vistusertib, demonstrating a strong response across the entire class (Figures 7C and S6B), in line with PIK3CA mutation driving the disease. However, distinct sensitivity to agents within the same drug class can occur. For instance, SARC0133, an RMS, showed the highest sensitivity to the fibroblast growth factor receptor (FGFR)-targeting drug infigratinib (Figure 7C). Sequencing revealed that SARC0133 harbors a FGFR1 gain on chromosome 8, contributing to its response (Figure 7A). Yet, there was minimal response to other FGFR-targeting molecules such as dovitinib (Figure S6C), which exemplify the ability of functional screening to differentiate activity of drugs within the same class.

The rapid turnover time of our screening platform can be leveraged for diagnostic purpose, particularly for well-defined genomic alterations linked to specific drug responses. For example, NTRK fusions drive responses to the FDA-approved NTRK inhibitor larotrectinib.[65,66] We received a diagnostic biopsy from a suspected infantile fibrosarcoma case, SARC0127‡. Fibrosarcoma harbors ETS variant transcription factor 6 (ETV6)-NTRK3 fusions in 90% of cases.[67,68] SARC0127‡ PDTOs were resistant to larotrectinib (Figure S6C, black arrowhead). Given the established link between NTRK alterations and larotrectinib sensitivity both in model systems and patients,[69] we hypothesized a different sarcoma subtype. Initial pathology suggested a high-grade sarcoma, with FISH results negative for ETV6 rearrangements. The tumor was ultimately diagnosed as high-grade spindle cell/sclerosing RMS, 18 days post-biopsy. Our platform provided diagnostic insights within a week, demonstrating its ability to quickly reveal tumor characteristics.

Comparison between PDTO and patient-derived xenografts

Sarcomas, particularly indolent ones, including many bone subtypes, are difficult to grow as patient-derived xenografts (PDXs), highlighting the need for organoids as pre-clinical models. We compared our PDTO screening results to 3 successfully established PDX models (Figure S7): an alveolar RMS (SARC0115), an Ewing sarcoma (SARC0111), and an epithelioid sarcoma (SARC0075). In the case of patient

(C) PDO viability scores for alpelisib and infigratinib. Black arrows indicate samples of interest.
(D) Correlation between osteosarcoma biopsy response to MAP and percent necrosis clinically determined at time of tumor resection post neo-adjuvant MAP treatment for the same patients.
(E) Comparison of PDTO performance and patient outcomes.
(F) Normalized time to next systemic therapy (TTNT) compared with PDO viability score for therapeutic regimens screened on organoids and administered to the patient immediately following sample procurement using simple linear regression. TTNT of the matching therapeutic regimen is normalized to the TTNT of the regimen used immediately preceding specimen collection. TTNT greater than 1 indicates that the treatment of interest yielded longer TTNT compared with the previously administered treatment. Sample diagnosis and therapeutic regimen are annotated for each point.
See also Figures S6 and S7.

SARC0115, we observed an excellent correlation between treatments identified as effective *ex vivo* in PDTOs and *in vivo* in PDXs, with vincristine, doxorubicin, cyclophosphamide (VDC) as the most effective regimen ($R^2 = 0.81$, $p = 0.04$; Figures S7A and S7B). PDXs from SARC0111 responded similarly to all treatments tested (Figure S7C). However, while 2/3 regimens showed comparable trends in PDTOs (doxorubicin, everolimus, and linsitib), one demonstrated a strong response in PDXs only (everolimus and lenvatinib, Figure S7D).

Lastly, we investigated SARC0075 due to the clinically observed heterogeneity in response. The behavior was well recapitulated in organoids established from 4 individual tumors obtained during the same surgery (Figures 3 and S7E). Heterogeneity was also evident at the genomic level: despite a very small number of common SNVs in pathogenic cancer drivers (ARID2, CRTC1, and MAP3K1), we identified several complex copy number variants (CNVs), including whole genome duplications and chromosome arm level gains and losses both at the clonal and subclonal level, which only partially overlapped between individual tumors (Figure S7F). While the PDXs established from a single separate tumor were responsive to temozolomide (Figure S7G), only 1/4 PDTO showed a statistically significant reduction in viability (Figures S7H and S7I). This case highlights one key advantage of PDTOs: they can be established from multiple tumor sites and screened rapidly in a cost-effective manner, which is particularly important to quantify tumor heterogeneity.

Evidence of correlation between PDTO and patient responses for matched treatment regimens

A major goal of developing personalized tumor organoid models is to leverage them to predict response to treatment. We have compared the PDTO screening results to clinical outcomes for 2 sets of samples (Figures 7D–7F). SARC0041‡, SARC0064‡, and SARC0135‡ are diagnostic biopsies from treatment-naive osteosarcoma patients. All patients received neo-adjuvant standard-of-care MAP between the time of biopsy and tumor resection. Upon resection, tumor tissue from SARC0041 and SARC0054 was found to be 99% and 95% necrotic, respectively, while SARC0135 had only 60% necrosis. Tumor necrosis post neo-adjuvant therapy is correlated to osteosarcoma clinical outcomes, with necrosis >90% at resection indicative of long-term responses.[70] *Ex vivo*, SARC0041‡ PDTOs had a 50% residual viability upon platinum treatment, while SARC0064‡ had 57% on MAP. Conversely, SARC0135‡ had a 73% residual viability post MAP treatment (Figures 7D and 7E). As indicated in Figure 7E, the two patients with stronger response *ex vivo* (SARC0041 and SARC0064) as measured by lower organoid viability % or AUC, have no evidence of tumor resurgence over 1,500 and 1,400 days post-surgery, respectively. The patient who had a significantly diminished *ex vivo* response to MAP (SARC0135) relapsed within 200 days from surgery. Thus, osteosarcoma organoid responses to neo-adjuvant therapy correlated to both short-term histologic response (necrosis at time of surgery) and long-term patient outcomes (progression-free survival).

We identified a small cohort of patients who immediately after surgery received a treatment regimen that was included in the library of compounds tested on the PDTOs. These include SARC0088, a patient with metastatic osteosarcoma treated with bortezomib and panobinostat; SARC0103, another metastatic osteosarcoma patient treated with gemcitabine and docetaxel; SARC0105, a primary osteosarcoma patient treated with gemcitabine and docetaxel; SARC0125, an RMS patient treated with mocetinostat and vinorelbine; and SARC0115, an RMS treated with irinotecan and temozolomide. While the sample size is limited ($n = 5$), we observed a correlation between normalized organoid viability and time to next treatment (TTNT) as a metric for real-world clinical response[71] ($R^2 = 0.921$, $p = 0.009$; Figure 7F). While further research with larger patient cohorts is warranted to validate these findings, the data supports the potential utility of PDTOs in predicting treatment response for sarcoma.

DISCUSSION

Sarcomas are rare cancers, accounting for less than 1% of annual cancer diagnoses[3] and encompassing over 100 subtypes. Some of these are indolent and hard to culture as cell lines or xenografts,[29] while others are exceedingly rare and understudied.[29] Clinically relevant disease models are lacking for most rare cancer subtypes.[72] We systematically explored drug sensitivity and resistance in sarcoma, including patients across 24 distinct histological subtypes at various disease stages and treatment histories. The organoids faithfully replicated the histological features of the original tumors, with unique characteristics in shape, aggregation patterns, and growth dynamics (Figure 2). This study demonstrates the feasibility of rapidly generating personalized organoid models from diverse rare sarcomas.

Patient-derived organoids are valuable for precision medicine due to their ability to replicate a patient's therapeutic response.[26,73] Incorporating organoid screening into clinical decision-making depends on the timing, reliability, and predictive accuracy of these tests. We demonstrate the feasibility of developing a translational pipeline for large-scale functional precision medicine within a single institution. This entailed developing protocols for patient identification, clinical data retrieval, tissue preservation post-surgery, and generating organoids for high-throughput screening, with results available within a week from procurement (Figure 1). Our finding that cryopreserved sarcoma tissue can produce viable organoids supports feasibility of cross-institutional programs.

Our pipeline's ability to screen drugs, including FDA-approved regimens or those in clinical trials, within a week of biopsy or surgery offers oncologists rapid actionable insights. Conventional precision medicine methods based on sequencing identify targetable alterations for ~30% of patients.[74] We quantified the "actionability" of the sarcoma mini-ring organoid platform, defining as actionable cases for which the 5 most effective regimens for which PDTOs are within the top 10% of responders are either FDA approved, NCCN recommended, or in trials. This approach identified at least one actionable option for 58% of patients screened, demonstrating the broad applicability of our functional precision medicine platform. Yet, while many identified drugs are FDA approved, fewer than 5% were approved for the specific cancer type diagnosed, and only 6% were listed in NCCN Guidelines (Figure 6B). Although standard therapies worked well in several cases (e.g., MAP or second-line therapies

for osteosarcoma, vinorelbine for RMS, or pazopanib for LMS), our analysis (Figure 6) suggests that some patients might respond better to FDA-approved treatments not typically considered for their cancer type. Access to such drugs will be a significant challenge in adopting functional precision medicine recommendations in clinical practice.

Tumor organoids have been shown to match clinical responses in a variety of carcinomas.[32,73,75] To evaluate the predictive power of sarcoma organoids, we determined concordance between organoid viability and clinical responses in 2 sets of samples. In the first, organoid responses to MAP therapy in three treatment-naive osteosarcoma biopsies correlated with clinically assessed necrosis post-neo-adjuvant therapy and long-term patient outcomes (Figures 7E and 7F).[71,76] We also explored correlations between organoid responses and TTNT, a real-life measure of therapy response. Given the heterogeneity of sarcoma clinical courses, therapies, and study inclusion times, progression-free survival or overall survival has limited interpretability. Therefore, we opted for TTNT, avoiding confounders by including only patients who progressed to the next therapy due to disease progression.[77,78] Despite the heterogeneities, we could detect a trend where patients whose organoids responded *ex vivo* had longer TTNT, and those with resistant organoids had shorter TTNT (Figure 7G). These results require validation in a larger cohort. Consequently, we initiated a clinical trial (NCT06064682: an organoid-based functional PREcision Medicine trial in OSTeosarcoma, PREMOST[79]) to confirm the feasibility of using our assay to predict therapy response to neo-adjuvant MAP in osteosarcoma (arm 1) and to investigate responses to FDA-approved drugs in advanced osteosarcoma (arm 2).

The goal of precision medicine, including organoid-based approaches, is to identify effective treatments, avoid ineffective ones, and improve outcomes. When combined with genomic analyses, these assays can help pinpoint the most effective molecule within a drug class (Figures 7A–7C and S6). PDTOs captured patient-to-patient heterogeneity observed in the clinic (Figures 3 and 7). For instance, we observed varying sensitivity to the multi-receptor tyrosine kinase inhibitor pazopanib in osteosarcoma organoids (Figure 3B). Clinically, pazopanib has shown partial response or stable disease in 13/19 (68%) metastatic osteosarcoma patients, with no biomarker available to stratify sensitive and resistant cases.[80,81]

Perhaps the biggest hurdle to precision medicine remains sampling bias, especially for highly heterogeneous sarcomas and advanced, disseminated disease. We found marked intra-patient heterogeneity (Figures 3, S7E, and S7F). This heterogeneity may be driven by complex genomic alterations (Figure S7F). While PDXs and PDTOs showed good correlation in some tumors, PDTOs afford the opportunity to model individual lesions or different areas within the same tumor, capturing intra-tumoral and intra-patient heterogeneity more effectively.

The landscape analysis of sarcoma drug response has utility beyond precision medicine applications. Our data highlighted unexplored relationships between drug sensitivity and clinical attributes such as histology, patient age, lesion type, and treatment history (Figure 4). We identified resistance patterns to drugs like rapamycin and shared sensitivities to sorafenib and ruxolitinib among patients with rapid disease progression (Figure 4). Identifying resistance or sensitivity patterns linked to clinical attributes will help delineate biomarkers for bone and soft tissue sarcomas.

Limitations of the study

Some advanced/metastatic tumors may have higher proliferation rates, potentially leading to increased drug sensitivity to a few agents, as we report. Our data lacks normalization for proliferation rates. Since our patient correlation data was collected for research, we lacked target lesions for RECIST evaluation and appropriate imaging. RECIST criteria usefulness has been called into question in sarcoma, as many of these tumors do not grow in similar patterns to carcinomas.[82,83] The non-spherical nature of most sarcomas, along with edema, fibrosis, necrosis, and intratumoral hemorrhage, may limit the effectiveness of conventional tumor size-based measures in distinguishing responders from non-responders. ^{18}F-FDG-PET, functional MRI, and patient-reported outcomes are possible alternatives,[82–85] which could be investigated in future studies investigating the correlation of sarcoma organoid responses to patient outcomes.

RESOURCE AVAILABILITY

Lead contact

Further requests for information or resources should be directed to the lead contact, Alice Soragni (alices@mednet.ucla.edu).

Materials availability

There are restrictions to the availability of residual sarcoma frozen cells due to the lack of an external centralized repository for their distribution and the need to maintain a stock. We are glad to share these when available with a completed materials transfer agreement.

Data and code availability

- RNA-seq raw data and corresponding metadata, DNA panel sequencing for the samples listed in Figures 2 and 7, and single-agent screening data shared in Figures 3 and 4 have been deposited on Synapse at: https://www.synapse.org/PDTOSarcoma. Archival DOIs are listed in the key resources table. The DNA panel sequencing data will also be shared through cBioPortal.
- Code for performing the machine learning-based image segmentation of bright-field images has been made public on GitHub (https://github.com/uclahs-soragnilab/Brightfield_Image_Segmentation_Quantification) and is publicly available as of the date of publication. An archival DOI is listed in the key resources table.
- Any additional information needed to re-analyze the data reported in this paper is available from the lead contact upon request.

ACKNOWLEDGMENTS

We acknowledge the UCLA Translational Pathology Core Laboratory for tissue procurement, the CAMD core at Dana-Farber for targeted sequencing, and Mark Duhon and UCLA's Technology Center for Genomics & Bioinformatics for help with RNA-seq. Thanks to Robert Damoiseaux and the UCLA MSSR Core for drug libraries and the UCLA JCCC BASE team for consultation on statistical analyses. We also thank Dr. Brian Kadera, Dr. Brooke Crawford, Dr. Jacquelyn Crane, Dr. Danielle S. Graham, Dr. Joseph K. Kendal, Dr. Benjamin J. DiPardo, and Matthew Mapua for their support with patient consenting, tissue collection or technical assistance. We are deeply grateful to the patients and families who participated in this study. This work was supported by NCI grants R01CA244729 and R01CA244729-03S1 (to A.S. and P.C.B.), a Slifka Foundation Award (to A.S. and N.C.F.), a UCLA DGSOM Seed Award (to A.S., P.C.B., N.C.F., A.K.K., and J.Y.), a JCCC Fellowship Award (to P.J.T.), NIH U24CA248265 (to P.C.B.), and a UCLA JCCC Program Leader Vision Award (to S.D.N.).

AUTHOR CONTRIBUTIONS

A.S. designed and supervised the project. S.D., A.S.S., B.C., J.G.C., A.K.K., F.C.E., F.H., N.M.B., N.C.F., and J.Y. consented the patients and obtained the surgical specimens. S.D.N. performed pathology assessments. A.A.S., P.J.T., H.T.L.N., S.S., and N.T. performed organoid establishment, characterization, and screening experiments. A.S., A.A.S., P.J.T., J.C., A.Y.J., M.D.-I. and H.C. performed organoid response data analyses. A.A.S., P.J.T., H.T.L.N., S.S., and N.T. performed immunohistochemistry experiments. A.D. and A.A.S. created the database of samples and drugs, performed the clustering analysis and pathway analysis, and generated visualizations. A.D. trained the neural net, and P.J.T. and A.A.S. performed the image segmentation experiment. A.E.G., H.W., S.T.F.-G., T.N.Y., and J.H.J. performed WGS data processing and analyses. A.A.S. and S.N. curated the clinical database. J.S. and J.N. performed *in vivo* experiments. A.A.S., P.J.T., and A.S. wrote the paper with contributions from all authors.

DECLARATION OF INTERESTS

A.S., J.Y., P.C.B., and N.C.F. are founders and owners of Icona BioDx. A.S. is a founder and owner of MiRiO.

STAR★METHODS

Detailed methods are provided in the online version of this paper and include the following:

- KEY RESOURCES TABLE
- EXPERIMENTAL MODEL AND STUDY PARTICIPANTS
  - Patients and samples' characteristics
  - Sample collection and processing
- METHOD DETAILS
  - Organoid Generation
  - Drug Screening
  - Histopathology
  - Targeted Sequencing
  - Whole Genome Sequencing
  - Fluorescence In Situ Hybridization (FISH)
  - RNAseq
  - PDX Model Establishment
  - *In Vivo* Pharmacology
- QUANTIFICATION AND STATISTICAL ANALYSIS
  - Database
  - Drug Screening Analysis
  - Quantification of samples with broad sensitivity
  - Growth Quantification with Image Analysis
  - Pathway Analysis
  - Assessment of Drug Availability

SUPPLEMENTAL INFORMATION

Supplemental information can be found online at https://doi.org/10.1016/j.stem.2024.08.010.

Received: August 16, 2023
Revised: June 14, 2024
Accepted: August 21, 2024
Published: September 20, 2024

REFERENCES

1. Mackall, C.L., Meltzer, P.S., and Helman, L.J. (2002). Focus on sarcomas. Cancer Cell *2*, 175–178.
2. Miller, R.W., Young, J.L., and Novakovic, B. (1995). Childhood cancer. Cancer *75*, 395–405.
3. Siegel, R.L., Miller, K.D., Fuchs, H.E., and Jemal, A. (2022). Cancer statistics, 2022. CA Cancer J. Clin. *72*, 7–33.
4. von Mehren, M., Kane, J.M., Agulnik, M., Bui, M.M., Carr-Ascher, J., Choy, E., Connelly, M., Dry, S., Ganjoo, K.N., Gonzalez, R.J., et al. (2022). Soft tissue sarcoma, version 2.2022, NCCN clinical practice guidelines in oncology. J. Natl. Compr. Canc. Netw. *20*, 815–833.
5. NCCN (2023). NCCN Guidelines Version 2. Bone Cancer. https://www.nccn.org/professionals/physician_gls/pdf/bone.pdf.
6. NIH (2020). SEER Cancer Statistics Review (CSR) 1975-2017. https://seer.cancer.gov/csr/1975_2017/index.html.
7. Rothzerg, E., Xu, J., and Wood, D. (2023). Different Subtypes of Osteosarcoma: Histopathological Patterns and Clinical Behaviour. J. Mol. Pathol. *4*, 99–108.
8. Perry, J.A., Seong, B.K.A., and Stegmaier, K. (2019). Biology and Therapy of Dominant Fusion Oncoproteins Involving Transcription Factor and Chromatin Regulators in Sarcomas. Annu. Rev. Cancer Biol. *3*, 299–321.
9. Damerell, V., Pepper, M.S., and Prince, S. (2021). Molecular mechanisms underpinning sarcomas and implications for current and future therapy. Signal Transduct. Target. Ther. *6*, 246.
10. Nacev, B.A., Sanchez-Vega, F., Smith, S.A., Antonescu, C.R., Rosenbaum, E., Shi, H., Tang, C., Socci, N.D., Rana, S., Gularte-Mérida, R., et al. (2022). Clinical sequencing of soft tissue and bone sarcomas delineates diverse genomic landscapes and potential therapeutic targets. Nat. Commun. *13*, 3405.
11. Steele, C.D., Tarabichi, M., Oukrif, D., Webster, A.P., Ye, H., Fittall, M., Lombard, P., Martincorena, I., Tarpey, P.S., Collord, G., et al. (2019). Undifferentiated Sarcomas Develop through Distinct Evolutionary Pathways. Cancer Cell *35*, 441–456.e8.
12. Taylor, B.S., Barretina, J., Maki, R.G., Antonescu, C.R., Singer, S., and Ladanyi, M. (2011). Advances in sarcoma genomics and new therapeutic targets. Nat. Rev. Cancer *11*, 541–557.
13. Carmagnani Pestana, R., Groisberg, R., Roszik, J., and Subbiah, V. (2019). Precision Oncology in Sarcomas: Divide and Conquer. JCO Precis. Oncol. *3*, 1–16.
14. McConnell, L., Houghton, O., Stewart, P., Gazdova, J., Srivastava, S., Kim, C., Catherwood, M., Strobl, A., Flanagan, A.M., Oniscu, A., et al. (2020). A novel next generation sequencing approach to improve sarcoma diagnosis. Mod. Pathol. *33*, 1350–1359.
15. Racanelli, D., Brenca, M., Baldazzi, D., Goeman, F., Casini, B., De Angelis, B., Guercio, M., Milano, G.M., Tamborini, E., Busico, A., et al. (2020). Next-Generation Sequencing Approaches for the Identification of Pathognomonic Fusion Transcripts in Sarcomas: The Experience of the Italian ACC Sarcoma Working Group. Front. Oncol. *10*, 489.
16. Flaherty, K.T., Gray, R., Chen, A., Li, S., Patton, D., Hamilton, S.R., Williams, P.M., Mitchell, E.P., Iafrate, A.J., Sklar, J., et al. (2020). The Molecular Analysis for Therapy Choice (NCI-MATCH) Trial: Lessons for Genomic Trial Design. J. Natl. Cancer Inst. *112*, 1021–1029.
17. Gounder, M.M., Agaram, N.P., Trabucco, S.E., Robinson, V., Ferraro, R.A., Millis, S.Z., Krishnan, A., Lee, J., Attia, S., Abida, W., et al. (2022). Clinical genomic profiling in the management of patients with soft tissue and bone sarcoma. Nat. Commun. *13*, 3406.
18. Lucchesi, C., Khalifa, E., Laizet, Y., Soubeyran, I., Mathoulin-Pelissier, S., Chomienne, C., and Italiano, A. (2018). Targetable Alterations in Adult Patients With Soft-Tissue Sarcomas: Insights for Personalized Therapy. JAMA Oncol. *4*, 1398–1404.
19. van der Graaf, W.T.A., Tesselaar, M.E.T., McVeigh, T.P., Oyen, W.J.G., and Fröhling, S. (2022). Biology-guided precision medicine in rare cancers: Lessons from sarcomas and neuroendocrine tumours. Semin. Cancer Biol. *84*, 228–241.
20. Nguyen, H.T.L., and Soragni, A. (2020). Patient-Derived Tumor Organoid Rings for Histologic Characterization and High-Throughput Screening. Star Protoc. *1*, 100056.
21. Vlachogiannis, G., Hedayat, S., Vatsiou, A., Jamin, Y., Fernández-Mateos, J., Khan, K., Lampis, A., Eason, K., Huntingford, I., Burke, R.,

et al. (2018). Patient-derived organoids model treatment response of metastatic gastrointestinal cancers. Science *359*, 920–926.

22. Hsu, K.-S., Adileh, M., Martin, M.L., Makarov, V., Chen, J., Wu, C., Bodo, S., Klingler, S., Sauvé, C.G., Szeglin, B.C., et al. (2022). Colorectal Cancer Develops Inherent Radiosensitivity That Can Be Predicted Using Patient-Derived Organoids. Cancer Res. *82*, 2298–2312.
23. van de Wetering, M., Francies, H.E., Francis, J.M., Bounova, G., Iorio, F., Pronk, A., van Houdt, W., van Gorp, J., Taylor-Weiner, A., Kester, L., et al. (2015). Prospective Derivation of a Living Organoid Biobank of Colorectal Cancer Patients. Cell *161*, 933–945.
24. Pasch, C.A., Favreau, P.F., Yueh, A.E., Babiarz, C.P., Gillette, A.A., Sharick, J.T., Karim, M.R., Nickel, K.P., DeZeeuw, A.K., Sprackling, C.M., et al. (2019). Patient-Derived Cancer Organoid Cultures to Predict Sensitivity to Chemotherapy and Radiation. Clin. Cancer Res. *25*, 5376–5387.
25. Ooft, S.N., Weeber, F., Dijkstra, K.K., McLean, C.M., Kaing, S., van Werkhoven, E., Schipper, L., Hoes, L., Vis, D.J., van de Haar, J., et al. (2019). Patient-derived organoids can predict response to chemotherapy in metastatic colorectal cancer patients. Sci. Transl. Med. *11*, eaay2574.
26. Yao, Y., Xu, X., Yang, L., Zhu, J., Wan, J., Shen, L., Xia, F., Fu, G., Deng, Y., Pan, M., et al. (2020). Patient-Derived Organoids Predict Chemoradiation Responses of Locally Advanced Rectal Cancer. Cell Stem Cell *26*, 17–26.e6.
27. Tiriac, H., Belleau, P., Engle, D.D., Plenker, D., Deschênes, A., Somerville, T.D.D., Froeling, F.E.M., Burkhart, R.A., Denroche, R.E., Jang, G.-H., et al. (2018). Organoid Profiling Identifies Common Responders to Chemotherapy in Pancreatic Cancer. Cancer Discov. *8*, 1112–1129.
28. Zhao, Z., Chen, X., Dowbaj, A.M., Sljukic, A., Bratlie, K., Lin, L., Fong, E.L.S., Balachander, G.M., Chen, Z., Soragni, A., et al. (2022). Organoids. Nat. Rev. Methods Primers *2*, 1–21.
29. Al Shihabi, A., Davarifar, A., Nguyen, H.T.L., Tavanaie, N., Nelson, S.D., Yanagawa, J., Federman, N., Bernthal, N., Hornicek, F., and Soragni, A. (2022). Personalized chordoma organoids for drug discovery studies. Sci. Adv. *8*, eabl3674.
30. Forsythe, S.D., Sivakumar, H., Erali, R.A., Wajih, N., Li, W., Shen, P., Levine, E.A., Miller, K.E., Skardal, A., and Votanopoulos, K.I. (2022). Patient-Specific Sarcoma Organoids for Personalized Translational Research: Unification of the Operating Room with Rare Cancer Research and Clinical Implications. Ann. Surg. Oncol. *29*, 7354–7367.
31. He, A., Huang, Y., Cheng, W., Zhang, D., He, W., Bai, Y., Gu, C., Ma, Z., He, Z., Si, G., et al. (2020). Organoid culture system for patient-derived lung metastatic osteosarcoma. Med. Oncol. *37*, 105.
32. Phan, N., Hong, J.J., Tofig, B., Mapua, M., Elashoff, D., Moatamed, N.A., Huang, J., Memarzadeh, S., Damoiseaux, R., and Soragni, A. (2019). A simple high-throughput approach identifies actionable drug sensitivities in patient-derived tumor organoids. Commun. Biol. *2*, 78.
33. Tebon, P.J., Wang, B., Markowitz, A.L., Davarifar, A., Tsai, B.L., Krawczuk, P., Gonzalez, A.E., Sartini, S., Murray, G.F., Nguyen, H.T.L., et al. (2023). Drug screening at single-organoid resolution via bioprinting and interferometry. Nat. Commun. *14*, 3168.
34. Nguyen, H.T.L., Kohl, E., Bade, J., Eng, S.E., Tosevska, A., Al Shihabi, A.A., Tebon, P.J., Hong, J.J., Dry, S., Boutros, P.C., et al. (2024). A platform for rapid patient-derived cutaneous neurofibroma organoid establishment and screening. Cell Rep. Methods *4*, 100772.
35. Ronneberger, O., Fischer, P., and Brox, T. (2015). U-Net: Convolutional Networks for Biomedical Image Segmentation. In Medical Image Computing and Computer-Assisted Intervention – MICCAI 2015 Lecture Notes in Computer Science., N. Navab, J. Hornegger, W.M. Wells, and A.F. Frangi, eds. (Springer International Publishing), pp. 234–241.
36. Iversen, P.W., Eastwood, B.J., Sittampalam, G.S., and Cox, K.L. (2006). A Comparison of Assay Performance Measures in Screening Assays: Signal Window, Z' Factor, and Assay Variability Ratio. J. Biomol. Screen. *11*, 247–252.
37. Atmaramani, R., Pancrazio, J.J., and Black, B.J. (2020). Adaptation of robust Z' factor for assay quality assessment in microelectrode array based screening using adult dorsal root ganglion neurons. J. Neurosci. Methods *339*, 108699.
38. Narasimhan, V., Wright, J.A., Churchill, M., Wang, T., Rosati, R., Lannagan, T.R., Vrbanac, L., Kobayashi, H., Richardson, A., Price, T., et al. (2020). Medium-throughput drug screening of patient-derived organoids from colorectal peritoneal metastases to direct personalized therapy. Clin. Cancer Res. Off. *26*, 3662–3670.
39. Said, R., and Tsimberidou, A.-M. (2022). Targeted Therapy in Cancer. In The MD Anderson Manual of Medical Oncology, H.M. Kantarjian, R.A. Wolff, and A.G. Rieber, eds. (McGraw Hill Education).
40. Dhall, G., Traverso, M., Finlay, J.L., Shane, L., Gonzalez-Gomez, I., and Jubran, R. (2011). The role of chemotherapy in pediatric clival chordomas. J. Neurooncol. *103*, 657–662.
41. Gelderblom, H., Hogendoorn, P.C.W., Dijkstra, S.D., van Rijswijk, C.S., Krol, A.D., Taminiau, A.H.M., and Bovée, J.V.M.G. (2008). The Clinical Approach Towards Chondrosarcoma. Oncologist *13*, 320–329.
42. Brahmi, M., Gaspar, N., Gantzer, J., Toulmonde, M., Boudou-Rouquette, P., Bompas, E., Firmin, N., Valentin, T., Cancel, M., Duffaud, F., et al. (2023). Patterns of care and outcome of CIC-rearranged sarcoma patients: A nationwide study of the French sarcoma group. Cancer Med. *12*, 7801–7807.
43. Federman, N., Crane, J., Gonzales, A.M., Arias, R., Baroudi, M., and Singh, A.S. (2022). A phase 1 dose-escalation/expansion clinical trial of mocetinostat in combination with vinorelbine in adolescents and young adults with refractory and/or recurrent rhabdomyosarcoma: Interim results. JCO *40*, 11553–11553. https://doi.org/10.1200/JCO.2022.40.16_suppl.11553.
44. Grünewald, T.G., Alonso, M., Avnet, S., Banito, A., Burdach, S., Cidre-Aranaz, F., Di Pompo, G., Distel, M., Dorado-Garcia, H., Garcia-Castro, J., et al. (2020). Sarcoma treatment in the era of molecular medicine. EMBO Mol. Med. *12*, e11131.
45. Stacchiotti, S., and Sommer, J.; Chordoma Global Consensus Group (2015). Building a global consensus approach to chordoma: a position paper from the medical and patient community. Lancet Oncol. *16*, e71–e83.
46. Walcott, B.P., Nahed, B.V., Mohyeldin, A., Coumans, J.-V., Kahle, K.T., and Ferreira, M.J. (2012). Chordoma: current concepts, management, and future directions. Lancet Oncol. *13*, e69–e76.
47. Sapkota, G.P., Cummings, L., Newell, F.S., Armstrong, C., Bain, J., Frodin, M., Grauert, M., Hoffmann, M., Schnapp, G., Steegmaier, M., et al. (2007). BI-D1870 is a specific inhibitor of the p90 RSK (ribosomal S6 kinase) isoforms in vitro and in vivo. Biochem. J. *401*, 29–38.
48. Miller, D.S., Blessing, J.A., Kilgore, L.C., Mannel, R., and Van Le, L. (2000). Phase II Trial of Topotecan in Patients With Advanced, Persistent, or Recurrent Uterine Leiomyosarcomas: A Gynecologic Oncology Group Study. Am. J. Clin. Oncol. *23*, 355–357.
49. Wolden, S.L., and Alektiar, K.M. (2010). Sarcomas Across the Age Spectrum. Semin. Radiat. Oncol. *20*, 45–51.
50. Smrke, A., Wang, Y., and Simmons, C. (2020). Update on Systemic Therapy for Advanced Soft-Tissue Sarcoma. Curr. Oncol. *27*, 25–33.
51. Li, C.H., Haider, S., and Boutros, P.C. (2022). Age influences on the molecular presentation of tumours. Nat. Commun. *13*, 208.
52. Martens, M., Ammar, A., Riutta, A., Waagmeester, A., Slenter, D.N., Hanspers, K., A Miller, R., Digles, D., Lopes, E.N., Ehrhart, F., et al. (2021). WikiPathways: connecting communities. Nucleic Acids Res. *49*, D613–D621.
53. Kanehisa, M., Furumichi, M., Sato, Y., Kawashima, M., and Ishiguro-Watanabe, M. (2023). KEGG for taxonomy-based analysis of pathways and genomes. Nucleic Acids Res. *51*, D587–D592.
54. Pakiet, A., Kobiela, J., Stepnowski, P., Sledzinski, T., and Mika, A. (2019). Changes in lipids composition and metabolism in colorectal cancer: a review. Lipids Health Dis. *18*, 29.

55. Seppälä, T.T., Zimmerman, J.W., Suri, R., Zlomke, H., Ivey, G.D., Szabolcs, A., Shubert, C.R., Cameron, J.L., Burns, W.R., Lafaro, K.J., et al. (2022). Precision medicine in pancreatic cancer: Patient derived organoid pharmacotyping is a predictive biomarker of clinical treatment response. Clin. Cancer Res. *28*, 3296–3307.

56. Sun, D., Gao, W., Hu, H., and Zhou, S. (2022). Why 90% of clinical drug development fails and how to improve it? Acta Pharm. Sin. B *12*, 3049–3062.

57. Beird, H.C., Bielack, S.S., Flanagan, A.M., Gill, J., Heymann, D., Janeway, K.A., Livingston, J.A., Roberts, R.D., Strauss, S.J., and Gorlick, R. (2022). Osteosarcoma. Nat. Rev. Dis. Primers *8*, 77.

58. Eisenhauer, E.A., Therasse, P., Bogaerts, J., Schwartz, L.H., Sargent, D., Ford, R., Dancey, J., Arbuck, S., Gwyther, S., Mooney, M., et al. (2009). New response evaluation criteria in solid tumours: Revised RECIST guideline (version 1.1). Eur. J. Cancer *45*, 228–247.

59. Grignani, G., Palmerini, E., Ferraresi, V., D'Ambrosio, L., Bertulli, R., Asaftei, S.D., Tamburini, A., Pignochino, Y., Sangiolo, D., Marchesi, E., et al. (2015). Sorafenib and everolimus for patients with unresectable high-grade osteosarcoma progressing after standard treatment: a non-randomised phase 2 clinical trial. Lancet Oncol. *16*, 98–107.

60. Dogruluk, T., Tsang, Y.H., Espitia, M., Chen, F., Chen, T., Chong, Z., Appadurai, V., Dogruluk, A., Eterovic, A.K., Bonnen, P.E., et al. (2015). Identification of Variant-Specific Functions of PIK3CA by Rapid Phenotyping of Rare Mutations. Cancer Res. *75*, 5341–5354.

61. Juric, D., Rodon, J., Tabernero, J., Janku, F., Burris, H.A., Schellens, J.H.M., Middleton, M.R., Berlin, J., Schuler, M., Gil-Martin, M., et al. (2018). Phosphatidylinositol 3-Kinase α-Selective Inhibition With Alpelisib (BYL719) in PIK3CA-Altered Solid Tumors: Results From the First-in-Human Study. J. Clin. Oncol. *36*, 1291–1299.

62. Maeda, M., Ochiai, K., Michishita, M., Morimatsu, M., Sakai, H., Kinoshita, N., Sakaue, M., Onozawa, E., Azakami, D., Yamamoto, M., et al. (2022). In vitro anticancer effects of alpelisib against PIK3CA-mutated canine hemangiosarcoma cell lines. Oncol. Rep. *47*, 1–9.

63. Juric, D., Janku, F., Rodón, J., Burris, H.A., Mayer, I.A., Schuler, M., Seggewiss-Bernhardt, R., Gil-Martin, M., Middleton, M.R., Baselga, J., et al. (2019). Alpelisib Plus Fulvestrant in PIK3CA-Altered and PIK3CA-Wild-Type Estrogen Receptor–Positive Advanced Breast Cancer: A Phase 1b Clinical Trial. JAMA Oncol. *5*, e184475.

64. André, F., Ciruelos, E., Rubovszky, G., Campone, M., Loibl, S., Rugo, H.S., Iwata, H., Conte, P., Mayer, I.A., Kaufman, B., et al. (2019). Alpelisib for PIK3CA-Mutated, Hormone Receptor–Positive Advanced Breast Cancer. N. Engl. J. Med. *380*, 1929–1940.

65. Gatalica, Z., Xiu, J., Swensen, J., and Vranic, S. (2019). Molecular characterization of cancers with NTRK gene fusions. Mod. Pathol. *32*, 147–153.

66. Davis, J.L., Lockwood, C.M., Albert, C.M., Tsuchiya, K., Hawkins, D.S., and Rudzinski, E.R. (2018). Infantile NTRK-associated Mesenchymal Tumors. Pediatr. Dev. Pathol. *21*, 68–78.

67. Knezevich, S.R., McFadden, D.E., Tao, W., Lim, J.F., and Sorensen, P.H.B. (1998). A novel ETV6-NTRK3 gene fusion in congenital fibrosarcoma. Nat. Genet. *18*, 184–187.

68. Bourgeois, J.M., Knezevich, S.R., Mathers, J.A., and Sorensen, P.H.B. (2000). Molecular Detection of the ETV6-NTRK3 Gene Fusion Differentiates Congenital Fibrosarcoma From Other Childhood Spindle Cell Tumors. Am. J. Surg. Pathol. *24*, 937–946.

69. Laetsch, T.W., DuBois, S.G., Mascarenhas, L., Turpin, B., Federman, N., Albert, C.M., Nagasubramanian, R., Davis, J.L., Rudzinski, E., Feraco, A.M., et al. (2018). Larotrectinib for paediatric solid tumours harbouring NTRK gene fusions: phase 1 results from a multicentre, open-label, phase 1/2 study. Lancet Oncol. *19*, 705–714.

70. Ferrari, S., Bacci, G., Picci, P., Mercuri, M., Briccoli, A., Pinto, D., Gasbarrini, A., Tienghi, A., and Brach del Prever, A. (1997). Long-term follow-up and post-relapse survival in patients with non-metastatic osteosarcoma of the extremity treated with neoadjuvant chemotherapy. Ann. Oncol. *8*, 765–771.

71. Campbell, B.A., Scarisbrick, J.J., Kim, Y.H., Wilcox, R.A., McCormack, C., and Prince, H.M. (2020). Time to Next Treatment as a Meaningful Endpoint for Trials of Primary Cutaneous Lymphoma. Cancers *12*, 2311.

72. Skubitz, K.M., Pambuccian, S., Manivel, J.C., and Skubitz, A.P.N. (2008). Identification of heterogeneity among soft tissue sarcomas by gene expression profiles from different tumors. J. Transl. Med. *6*, 23.

73. Guillen, K.P., Fujita, M., Butterfield, A.J., Scherer, S.D., Bailey, M.H., Chu, Z., DeRose, Y.S., Zhao, L., Cortes-Sanchez, E., Yang, C.-H., et al. (2022). A human breast cancer-derived xenograft and organoid platform for drug discovery and precision oncology. Nat. Cancer *3*, 232–250.

74. AACR Project GENIE Consortium (2017). AACR Project GENIE: Powering Precision Medicine through an International Consortium. Cancer Discov. *7*, 818–831.

75. Mäkinen, L., Vähä-Koskela, M., Juusola, M., Mustonen, H., Wennerberg, K., Hagström, J., Puolakkainen, P., and Seppänen, H. (2022). Pancreatic Cancer Organoids in the Field of Precision Medicine: A Review of Literature and Experience on Drug Sensitivity Testing with Multiple Readouts and Synergy Scoring. Cancers *14*, 525.

76. Tsuda, Y., Tsoi, K., Parry, M.C., Stevenson, J.D., Fujiwara, T., Sumathi, V., and Jeys, L.M. (2020). Impact of chemotherapy-induced necrosis on event-free and overall survival after preoperative MAP chemotherapy in patients with primary high-grade localized osteosarcoma. Bone Joint. J. *102-B*, 795–803.

77. Coleman, R.L., Salani, R., Boyle, T., Perhanidis, J., Lim, J., Kalilani, L., Schilder, J.M., Hurteau, J., Golembesky, A., and Backes, F. (2023). 43P Time to next treatment (TTNT) of first-line maintenance (1Lm) niraparib monotherapy in epithelial ovarian cancer (EOC) patients (pts) in the CHAR1ZMA study. ESMO Open *8*.

78. Walker, B., Boyd, M., Aguilar, K., Davies, K., Espirito, J., Frytak, J., and Robert, N. (2021). Comparisons of Real-World Time-to-Event End Points in Oncology Research. JCO Clin. Cancer Inform. *5*, 45–46.

79. ClinicalTrials.gov. An organoid-based functional precision medicine trial in osteosarcoma. https://clinicaltrials.gov/study/NCT06064682.

80. Aggerholm-Pedersen, N., Rossen, P., Rose, H., and Safwat, A. (2020). Pazopanib in the Treatment of Bone Sarcomas: Clinical Experience. Transl. Oncol. *13*, 295–299.

81. Pillozzi, S., Bernini, A., Palchetti, I., Crociani, O., Antonuzzo, L., Campanacci, D., and Scoccianti, G. (2021). Soft Tissue Sarcoma: An Insight on Biomarkers at Molecular, Metabolic and Cellular Level. Cancers *13*, 3044.

82. Schuetze, S.M., Baker, L.H., Benjamin, R.S., and Canetta, R. (2008). Selection of Response Criteria for Clinical Trials of Sarcoma Treatment. Oncologist *13*, 32–40.

83. Kim, A., Lu, Y., Okuno, S.H., Reinke, D., Maertens, O., Perentesis, J., Basu, M., Wolters, P.L., De Raedt, T., Chawla, S., et al. (2020). Targeting Refractory Sarcomas and Malignant Peripheral Nerve Sheath Tumors in a Phase I/II Study of Sirolimus in Combination with Ganetespib (SARC023). Sarcoma *2020*, 5784876.

84. Herrmann, K., Benz, M.R., Czernin, J., Allen-Auerbach, M.S., Tap, W.D., Dry, S.M., Schuster, T., Eckardt, J.J., Phelps, M.E., Weber, W.A., and Eilber, F.C. (2012). 18F-FDG-PET/CT Imaging as an Early Survival Predictor in Patients with Primary High-Grade Soft Tissue Sarcomas Undergoing Neoadjuvant Therapy. Clin. Cancer Res. *18*, 2024–2031.

85. Soldatos, T., Ahlawat, S., Montgomery, E., Chalian, M., Jacobs, M.A., and Fayad, L.M. (2016). Multiparametric Assessment of Treatment Response in High-Grade Soft-Tissue Sarcomas with Anatomic and Functional MR Imaging Sequences. Radiology *278*, 831–840.

86. American Cancer Society. Cancer Facts & Figures 2024. https://www.cancer.org/research/cancer-facts-statistics/all-cancer-facts-figures/2024-cancer-facts-figures.html.

87. de Pinieux, G., Karanian, M., Le Loarer, F., Le Guellec, S., Chabaud, S., Terrier, P., Bouvier, C., Batistella, M., Neuville, A., Robin, Y.-M., et al. (2021). Nationwide incidence of sarcomas and connective tissue tumors

of intermediate malignancy over four years using an expert pathology review network. PLoS One *16*, e0246958.

88. Garcia, E.P., Minkovsky, A., Jia, Y., Ducar, M.D., Shivdasani, P., Gong, X., Ligon, A.H., Sholl, L.M., Kuo, F.C., MacConaill, L.E., et al. (2017). Validation of OncoPanel: A Targeted Next-Generation Sequencing Assay for the Detection of Somatic Variants in Cancer. Arch. Pathol. Lab. Med. *141*, 751–758.
89. Vasimuddin, M., Misra, S., Li, H., and Aluru, S. (2019). Efficient Architecture-Aware Acceleration of BWA-MEM for Multicore Systems. Preprint at arXiv. https://doi.org/10.48550/arXiv.1907.12931.
90. Danecek, P., Bonfield, J.K., Liddle, J., Marshall, J., Ohan, V., Pollard, M.O., Whitwham, A., Keane, T., McCarthy, S.A., Davies, R.M., and Li, H. (2021). Twelve years of SAMtools and BCFtools. GigaScience *10*, giab008.
91. McKenna, A., Hanna, M., Banks, E., Sivachenko, A., Cibulskis, K., Kernytsky, A., Garimella, K., Altshuler, D., Gabriel, S., Daly, M., and DePristo, M.A. (2010). The Genome Analysis Toolkit: A MapReduce framework for analyzing next-generation DNA sequencing data. Genome Res. *20*, 1297–1303.
92. Benjamin, D., Sato, T., Cibulskis, K., Getz, G., Stewart, C., and Lichtenstein, L. (2019). Calling Somatic SNVs and Indels with Mutect2. Preprint at bioRxiv. https://doi.org/10.1101/861054.
93. Fan, Y., Xi, L., Hughes, D.S.T., Zhang, J., Zhang, J., Futreal, P.A., Wheeler, D.A., and Wang, W. (2016). MuSE: accounting for tumor heterogeneity using a sample-specific error model improves sensitivity and specificity in mutation calling from sequencing data. Genome Biol. *17*, 178.
94. Larson, D.E., Harris, C.C., Chen, K., Koboldt, D.C., Abbott, T.E., Dooling, D.J., Ley, T.J., Mardis, E.R., Wilson, R.K., and Ding, L. (2012). SomaticSniper: identification of somatic point mutations in whole genome sequencing data. Bioinformatics *28*, 311–317.
95. Kim, S., Scheffler, K., Halpern, A.L., Bekritsky, M.A., Noh, E., Källberg, M., Chen, X., Kim, Y., Beyter, D., Krusche, P., and Saunders, C.T. (2018). Strelka2: fast and accurate calling of germline and somatic variants. Nat. Methods *15*, 591–594.
96. Nik-Zainal, S., Van Loo, P., Wedge, D.C., Alexandrov, L.B., Greenman, C.D., Lau, K.W., Raine, K., Jones, D., Marshall, J., Ramakrishna, M., et al. (2012). The Life History of 21 Breast Cancers. Cell *149*, 994–1007.
97. Van Loo, P., Nordgard, S.H., Lingjærde, O.C., Russnes, H.G., Rye, I.H., Sun, W., Weigman, V.J., Marynen, P., Zetterberg, A., Naume, B., et al. (2010). Allele-specific copy number analysis of tumors. Proc. Natl. Acad. Sci. USA *107*, 16910–16915.
98. Patel, Y., Zhu, C., Yamaguchi, T.N., Bugh, Y.Z., Tian, M., Holmes, A., Fitz-Gibbon, S.T., and Boutros, P.C. (2024). NFTest: automated testing of Nextflow pipelines. Bioinformatics *40*, btae081.
99. Di Tommaso, P., Chatzou, M., Floden, E.W., Barja, P.P., Palumbo, E., and Notredame, C. (2017). Nextflow enables reproducible computational workflows. Nat. Biotechnol. *35*, 316–319.
100. Howie, B.N., Donnelly, P., and Marchini, J. (2009). A Flexible and Accurate Genotype Imputation Method for the Next Generation of Genome-Wide Association Studies. PLoS Genet. *5*, e1000529.
101. Dobin, A., Davis, C.A., Schlesinger, F., Drenkow, J., Zaleski, C., Jha, S., Batut, P., Chaisson, M., and Gingeras, T.R. (2013). STAR: ultrafast universal RNA-seq aligner. Bioinformatics. *29*, 15–21.
102. Partek, an Illumina company (2024). PartekTM Genomics SuiteTM, [Version 7.0].
103. Love, M.I., Huber, W., and Anders, S. (2014). Moderated estimation of fold change and dispersion for RNA-seq data with DESeq2. Genome Biol. *15*, 550.
104. Kim, S., Chen, J., Cheng, T., Gindulyte, A., He, J., He, S., Li, Q., Shoemaker, B.A., Thiessen, P.A., Yu, B., et al. (2021). PubChem in 2021: new data content and improved web interfaces. Nucleic Acids Res. *49*, D1388–D1395.
105. Zhang, J.H., Chung, T.D.Y., and Oldenburg, K.R. (1999). A Simple Statistical Parameter for Use in Evaluation and Validation of High Throughput Screening Assays. J. Biomol. Screen. *4*, 67–73.
106. He, K., Zhang, X., Ren, S., and Sun, J. (2016). Deep Residual Learning for Image Recognition. In 2016 IEEE Conference on Computer Vision and Pattern Recognition (CVPR), pp. 770–778.
107. Deng, J., Dong, W., Socher, R., Li, L.-J., Li, K., and Fei-Fei, L. (2009). ImageNet: A large-scale hierarchical image database. In 2009 IEEE Conference on Computer Vision and Pattern Recognition, pp. 248–255.

STAR★METHODS

KEY RESOURCES TABLE

REAGENT or RESOURCE	SOURCE	IDENTIFIER
Biological samples		
Human tumor samples	Patients included in this study	N/A
Chemicals, peptides, and recombinant proteins		
MammoCult™ Human Medium Kit	Stemcell Technologies	Ca#05620
Hydrocortisone Stock Solution	Stemcell Technologies	Ca#07925
Heparin Solution	Stemcell Technologies	Ca#07980
Matrigel Basement Membrane Matrix	Corning	Ca#354234
Collagenase type IV	Thermo Fisher	Ca#17-104-019
Dispase	Life Technologies	Ca#17105-041
Histogel	Thermo Fisher	Ca#R904012
Ammonium Chloride Solution	Stemcell Technologies	Ca#07850
Hanks' Balanced Salt Solution (HBSS)	Stemcell Technologies	Ca#37150
Cryostor®CS10	Sigma Aldrich	Ca#C2874
Recovery™ Cell Culture Freezing Medium	Thermo Fisher	Ca#12648010
Critical commercial assays		
CellTiter-Glo 3D	Promega	Ca#G968B
Deposited data		
RNA Sequencing (RNASeq) Raw Data Files (fastq)	Synapse: https://doi.org/10.7303/syn61892352	syn61892352
Targeted DNA sequencing (Figures 2 and 7): Sample info	Synapse: https://doi.org/10.7303/syn61894699	syn61894699
Targeted DNA sequencing (Figures 2 and 7): SNV	Synapse: https://doi.org/10.7303/syn61894695	syn61894695
Targeted DNA sequencing (Figures 2 and 7): SV	Synapse: https://doi.org/10.7303/syn61894696	syn61894696
Targeted DNA sequencing (Figures 2 and 7): CNV	Synapse: https://doi.org/10.7303/syn61894697	syn61894697
Viability scores (Figures 3 and 4)	Synapse: https://doi.org/10.7303/syn61892224	syn61892224
Software and algorithms		
Celigo S Software	Nexcelom	N/A
Brightfield_Image_Segmentation_Quantification	uclahs-soragnilab	https://github.com/uclahs-soragnilab/Brightfield_Image_Segmentation_Quantification
Prism 9.4.1 (681)	GraphPad	N/A
Illustrator (v28.4.1)	Adobe	N/A

EXPERIMENTAL MODEL AND STUDY PARTICIPANTS

Patients and samples' characteristics

Fresh tumor specimens are obtained from consenting patients (UCLA IRB #10-001857, 11-003254, 19-002214). Patient and sample demographics are outlined in Figure 1. Briefly, we included biopsies (n=11) and surgical resections (n=183) of primary, recurrent, and metastatic lesions. The patient population was majority adult at time of diagnosis (n=63/126) with 35% adolescent and young adults (AYA, n=45/126) and 13% pediatric patients (n=18/126). Sex distribution was 62% male (78/126) and 38% female (48/126), which resembles the proportion of incidence of bone and soft tissue sarcomas in the United States (57% male, 43% female).[86] 15% identified as Asian, 5% as Black, 1% as Pacific Islander/Samoan and 18% as Other. This study includes 24 distinct subtypes of bone and soft tissue sarcomas, with osteosarcoma being the most common (73 samples from 28 patients), followed by chordoma (14 samples from 10 patients) and chondrosarcoma (13 samples from 12 patients). For soft tissue sarcomas, leiomyosarcoma (12 samples from 10 patients) and undifferentiated pleomorphic sarcoma (11 samples from 10 patients) were predominant. The proportion of patients enrolled reflects the proportional incidences of the major sarcoma subtypes, with the exceptions of chordoma (overrepresented in our study) and leiomyosarcoma (underrepresented in our study).[87] The sample distribution was 46% metastases, 41% primary

tumors, and 13% recurrent tumors. Multiple specimens were collected from 27 patients (21%), either from different anatomical locations (12/27), longitudinally (21/27) or both (6/27). Most samples (71%) had been exposed to systemic therapies, with 23% (45/194) treated with three or more prior regimens, and 30% had a history of radiation. The median interval between the last systemic treatment and sample collection was one month for the 137 pre-treated specimens (range: 1-480 months) and 12 months for the 59 irradiated samples (range: 1-384 months). The treatment modalities varied by sarcoma subtype, reflecting the heterogeneity in clinical management.[4,5]

Sample collection and processing

The protocol for collecting and processing tumor tissue has been previously described.[20,29,32] Resected tumor specimens are routed to the Translational Pathology Laboratory Core at UCLA (TPCL) where they are grossed and are placed in RPMI solution for transfer to the laboratory. We request to avoid tissue marked with ink, and to avoid periphery as well as any obviously necrotic component. Solid tumors are minced manually with a scalpel and digested with collagenase IV (200 U/mL) to yield a suspension of single cells/small clusters. The cells are then transferred to a new tube, followed by red blood cell lysis with Ammonium Chloride Solution (Stem Cell Technology). Cells are then strained using a 100μm filter before counting and viability assessment using a Cellometer Auto 2000 (Nexcelom).

METHOD DETAILS

Organoid Generation

Primary cells are resuspended in a 3:4 solution of Mammocult medium (Stem Cell Technology) and Matrigel (Corning).[20,29,32] The mixture is kept on ice throughout the organoid seeding process to prevent premature crosslinking. We seed the organoids for drug screening by distributing 10μL of solution around the perimeter of the bottom of each well of a 96-well plate. We incubate the material for 30 minutes at 37°C to solidify the gel before adding 100μL of Mammocult medium to each well. Organoids cultured for histological and molecular analyses are seeded in 24-well plates. We seed 100,000 cells in 70μL of the Mammocult-Matrigel solution around the perimeter of each well of a 24-well plate. Each well plate is imaged using a high-content microscope (Celigo, Nexcelom) every 24 hours.

Drug Screening

After allowing the organoids to grow and develop for 3 days, we perform drug treatments using a panel of targeted agents and chemotherapies to assess sensitivity following our published protocols.[20,29,32–34] First, we remove the medium from each well using an automated fluid handler (Microlab NIMBUS, Hamilton or epMotion 96, Eppendorf) and replace it with pre-warmed Mammocult containing the desired drug concentration and 1% DMSO. Each plate contains its own positive and negative controls for normalization. The positive control is 10 μM staurosporine and the negative control is 1% DMSO. Organoids are incubated at 37°C and 5% CO_2 throughout drug treatment. After 24 hours, we exchange the medium with fresh, drug-loaded medium. After 2 days of treatment total, organoid viability is assessed with an ATP assay (CellTiter-Glo, Promega). The organoids are released from the matrix with dispase followed by addition of the CellTiter-Glo reagent. After 30 minutes, luminescence is measured using a SpectraMax iD3 plate reader (Molecular Devices).

Histopathology

Histopathology analysis is performed on the tissue of origin and the organoids derived from the collected specimens. Organoids are prepared for histopathology after 5 days of culture. Each well is washed with 1 mL of phosphate buffered saline (PBS) prior to fixation with 500 μL of 10% buffered formalin (VWR, 89379-094). After at least 24 hours of fixation, the organoids are removed from the 24-well plate and transferred to a conical tube. They are washed with PBS prior to the addition of 5 μL of Histogel (Thermo Fisher Scientific, HG-40000-012). The sample in Histogel is then transferred to a cassette and paraffin embedded. We section organoid blocks at 8 μm and mount them on Superfrost Plus Microscope Slides (12-550-15, Fisher Scientific). Hematoxylin and eosin staining was performed on the parent tumor and the resulting organoids derived from tissue collection according to standard protocols. All images were acquired using the Revolve Upright and Inverted Microscope System (Echo Laboratories).

Targeted Sequencing

Select samples are sent to the Center for Advanced Molecular Diagnostics (CAMD) at Brigham and Women's Hospital for analysis using the OncoPanel v3.[88] Sequencing was performed on pre-sectioned 10 slides from non-decalcified FFPE tissue blocks. Slides are then shipped to CAMD for sequencing and analysis. We plotted the results in a circos plot using R.

Whole Genome Sequencing

Sequencing reads were aligned to the GRCh38 reference build using BWA-MEM2 (v2.2.1)[89] in paired-end, alt-aware mode, sorted with SAMtools (v1.18)[90] followed by the Genome Analysis Toolkit (GATK) MarkDuplicatesSpark (v4.2.4.1).[91] Indel realignment and base quality score recalibration were performed using GATK IndelRealigner (v3.7.0)[91] and BaseRecalibrator (v4.2.4.1),[91] respectively. Somatic SNVs were called on tumor-normal pairs using four different algorithms, all with recommended default parameters: MuSE (v2.0.4), Mutect2 (v4.2.4.1),[92,93] SomaticSniper (v1.0.5.0),[94] and Strelka2 (v2.9.10).[95] The resulting variants were intersected

with BCFtools (v1.17)[90] and filtered to keep only somatic SNVs found by two or more callers. Somatic copy number alterations (sCNAs) in the tumor samples were identified using Battenberg (v2.2.9),[96] which was run using developer recommended parameters for WGS, with ASCAT (v3.1.2),[97] alleleCounter (v4.3.0; https://github.com/cancerit/alleleCount) and impute (v2.3.2). All alignment and variant calling operations were run on a Slurm high-performance computing cluster using Nextflow (v23.04.2)[98–100] pipelines (e.g. https://github.com/uclahs-cds/pipeline-call-sSNV) to ensure reproducibility and compatibility across computing environments.

Fluorescence In Situ Hybridization (FISH)

Identification of NTRK 1, 2, or 3 fusions was performed by preforming Fluorescence In Situ Hybridization (FISH). Slides from non-decalcified FFPE tissue blocks from select samples are sent to NeoGenomics for performing their NTRK 1, 2, 3 FISH Panel (#88374). Similarly, identification of MDM2 amplification was performed by NeoGenomics using a MDM2/CEN12 probe set (CEN12x1.7,MDM2x7.5. #88377), with a sample considered positive for MDM2 amplification when the MDM2/CEN12 ratio is $\geq$ 2 or over 12 copies of MDM2/cell are found on average.

RNAseq

Libraries for RNA-Seq were prepared with KAPA mRNA-Seq Hyper Prep Kit. The workflow consists of mRNA enrichment and fragmentation, first strand cDNA synthesis using random priming followed by second strand synthesis converting cDNA:RNA hybrid to double-stranded cDNA (dscDNA), and incorporates dUTP into the second cDNA strand. cDNA generation is followed by end repair to generate blunt ends, A-tailing, adaptor ligation and PCR amplification. Different adaptors were used for multiplexing samples in one lane. Sequencing was performed on Illumina NovaSeq6000 for a PE 2x150 run. Data quality check was done on Illumina SAV. Demultiplexing was performed with Illumina BCL Convert v4.2.7 software. The reads were mapped by STAR 2.7.9a[101] and read counts per gene were quantified using the human genome GRCh38. In Partek Flow, read counts were normalized by median ratio.[102,103] Spearman's rank correlation was calculated pairwise using the normalized read counts for each sample in the dataset.

PDX Model Establishment

All animal studies were conducted with institutional oversight under an IACUC-approved protocol at Certis Oncology Solutions, Inc. using adult female NOG mice (Taconic Biosciences, Germantown, NY, USA). Animals were shaved and surgically prepped using 70% isopropyl alcohol and surgical scrub. Fresh tissue samples were fragmented into approximately 8 mm3 pieces and implanted into the subcutaneous flanks of NOG mice. Tumor volumetric measurements were recorded twice weekly using standard caliper procedures and calculated by the formula 0.5 x L x W2. Body weights were also measured twice weekly throughout the length of the studies. Tumors were serially passaged into test animals once they reached 1000 mm3.

In Vivo Pharmacology

PDX tumors were surgically implanted orthotopically into the hind limbs of test animals to correspond with patient biopsy sites. Tumors were monitored weekly using T2 weighted (T2W) contrast on the M3 Compact MRI (1 Tesla) (Aspect Imaging, Nashville, TN, USA). Tumor volumes were quantified using VivoQuant software (Version 2021, Invicro, Needham, MA, USA). When tumors reached an average volume of 100 mm3, animals were randomized into study groups. Test agents were formulated and dosed according to manufacturer's instructions (MedChemExpress, Monmouth Junction, NJ, USA), and administered over a period of 4 weeks.

QUANTIFICATION AND STATISTICAL ANALYSIS

Database

We maintain a PostgreSQL relational database that stores coded non-identifiable patient and sample information of our biobank. We implemented several external databases to our database such as gene pathway data from WikiPathways,[52] and mechanistic targets of our drug library from PubChem[104] and literature. After organoid plates undergo drug screening, we use a Python-based, custom XML parser to upload the luminescence data to the database. This data is then connected to additional information about the patient and sample procurement using Django, a Python-based web framework. The drug treatment used for each well is also uploaded to the database. All downstream analysis is performed using R (v4.2) and begins by querying the database.

Drug Screening Analysis

We screened each drug with either n = 1 or 2 at a concentration of 1 μM if screened at single concentration or 0.1–10 μM for dose-concentration curves. Platinum agents, cisplatin and carboplatin, were screened at 25 and/or 50 μM as single agents and 25–100 μM for dose-concentration studies. Plate-level statistics including the Z'-factor,[105] and robust Z'-factor,[37] are calculated for each plate of organoids and are used as inclusion metrics for subsequent analysis. The thresholds for inclusion in this study are the following: Z'-factor $\geq$ 0.2 or robust Z'-factor $\geq$ 0.2. These criteria were selected to exclude plates that have an insufficient statistical effect size which are prone to false positives and negatives in high-throughput assays. We also excluded plates of experiments from passages or thawed samples if they were performed for the purpose of re-screening except for one sample where we included both the fresh and thawed experiment plates due to low QC metrics from the fresh experiment. We also excluded one sample from the analysis due to it being a benign tumor. We used the luminescence values of staurosporine screened at 10 μM as a positive control and substituted with 1 μM when not available. For plates that were screened with only one well of staurosporine 1 μM, the values were

pooled across the plates as a positive control for the experiment. For plates that were included in the analysis, the luminescence measurements from the ATP assay are normalized to the mean luminescence of the negative control (1% DMSO) wells to calculate percent viability. For each drug treatment, the viability of each sample is normalized to the mean response of all samples treated with the drug of interest to calculate the viability score. Response rank percentile is calculated by dividing the rank of each sample and dividing it by the total number of samples screened with each drug.

Quantification of samples with broad sensitivity

A subset of our samples showed broad sensitivity across many of the drug regimens screened. To identify these, we considered only samples with 10 or more distinct therapies tested. For each drug that was screened on at least 3 samples, we identified the samples in the top 5% of responders, the samples most responsive to each treatment. For each sample, we counted the number of drugs for which it appeared among the top 5% most sensitive samples. This number was then normalized to the number of total drugs screened on the sample to yield a proportion of drugs screened showing high sensitivity. Samples with broad sensitivity were defined as samples with more than 25% of the tested therapies showing high sensitivity.

Growth Quantification with Image Analysis

We image the organoids daily using a high-content microscope that scans two focal planes per well. The resulting whole-well images are exported in TIF format at a resolution of 1 μm/pixel. We then implement our previously developed methodology to segment and quantify regions of the image containing organoids.[29] We use a convolutional neural network with a U-Net architecture[35] to segment the regions of the images containing organoids. This model is based on a ResNet-34 model[106] trained on 223 manually labelled images spanning an array of tumors of origin to capture the diverse organoid morphologies observed in this study. In the manually labelled dataset, only in-focus organoids are marked for inclusion in the area calculation; this is done to minimize measuring the same organoid across both focal planes. The original weights were derived from a model pretrained on the ImageNet dataset[107] and the final model was trained over 80 epochs using a cross-entropy loss function. The trained model was then used to segment each image by splitting the image into 512x512 pixel sections, applying the model to each section, and reassembling the sections to recreate the whole segmented image (16,896x16896 pixels). We then implement OpenCV to calculate the total area of the organoids in each focal plane. This area is then averaged across both focal planes and growth is measured by normalizing to the area covered by organoids on the first day of imaging of the same well. The resulting data was then plotted using GraphPad Prism as normalized area over time.

Pathway Analysis

Protein targets for each drug in our library were annotated and obtained from PubChem[104] and literature. We selected only targets that are within 10-fold of the second-lowest reported value for Kd (dissociation constant) or IC50 (median inhibitory concentration) among the targets. To perform the pathway analysis, we mapped each drug and their protein target with values of 0 and 1, with 1 indicating that a drug targets a protein, and 0 indicating the lack of protein among the drug targets.[29] We filled the values in a matrix composed of n_{drugs} x $m_{protein}$. To adjust for the degree of impact of protein targets on the viability of samples, we multiplied each row in the matrix by a weight proportional to the mean viability of the organoids treated by each drug [1 − (mean viability/100)]. We then multiplied this matrix by a vector of 1s to obtain a row-wise summation of the protein target viability values. To adjust for protein targets that are targeted by multiple drugs in our library compared to targets associated with drugs that are less represented in our panels, we normalized the row vector by dividing each element by the sum of non-zero column entries in the $n_{drugs} \times m_{protein}$ matrix. We then mapped this list of proteins to the canonical pathways defined by the WikiPathways Database [version 20220710].[52] We excluded pathways that are not biologically pertinent to cancer, such pathways related to microorganisms and pathogens, as well as the newly added coronavirus disease (COVID)–related pathways. We populated a new matrix comprised of $n_{pathway}$ x $m_{protein}$, with 1s indicating the presence of a protein in a particular pathway or 0s indicating its absence. We then normalized the rows in the pathway matrix to account for the differences in the number of proteins included in each pathway. To obtain the relative effect that targeting a specific pathway has on the viability of sarcoma organoids, we multiplied the $n_{pathway} \times m_{protein}$ mapping matrix by the normalized $n_{drugs} \times m_{protein}$ vector. The resulting vector represents the relative impact that targeting a given pathway has on the viability of the organoids. We then ranked the scored pathways for each sample to compare the impact of each pathway on a viability of a sample between organoids of different sarcoma subtypes.[29]

Assessment of Drug Availability

Based on our drug screening data, we created a list of the five most effective therapeutic agents for each sample screened. We then created a second list of the top 10% most responsive samples to each drug. We considered only sample-drug pairs that appeared in both lists for further analysis and mapped each sample to its diagnostic subtype. For each drug-diagnosis pair, we manually annotated the inclusion of each therapy in the NCCN Guidelines[4,5] as well as the current FDA approval status for each drug with respect to the histological subtype.